Cell

Serpins Promote Cancer Cell Survival and Vascular Co-Option in Brain Metastasis

Manuel Valiente,[1] Anna C. Obenauf,[1] Xin Jin,[1] Qing Chen,[1] Xiang H.-F. Zhang,[1,8] Derek J. Lee,[1] Jamie E. Chaft,[2] Mark G. Kris,[2] Jason T. Huse,[3,4] Edi Brogi,[5] and Joan Massagué[1,4,6,7,*]
[1]Cancer Biology and Genetics Program
[2]Department of Medicine
[3]Human Oncology and Pathogenesis Program
[4]Brain Tumor Center
[5]Department of Pathology
[6]Metastasis Research Center
Memorial Sloan Kettering Cancer Center, New York, NY 10065, USA
[7]Howard Hughes Medical Institute, Chevy Chase, MD 21205, USA
[8]Present address: Lester and Sue Smith Breast Center, Baylor College of Medicine, One Baylor Plaza, Houston, TX 77030, USA
*Correspondence: j-massague@ski.mskcc.org
http://dx.doi.org/10.1016/j.cell.2014.01.040

SUMMARY

Brain metastasis is an ominous complication of cancer, yet most cancer cells that infiltrate the brain die of unknown causes. Here, we identify plasmin from the reactive brain stroma as a defense against metastatic invasion, and plasminogen activator (PA) inhibitory serpins in cancer cells as a shield against this defense. Plasmin suppresses brain metastasis in two ways: by converting membrane-bound astrocytic FasL into a paracrine death signal for cancer cells, and by inactivating the axon pathfinding molecule L1CAM, which metastatic cells express for spreading along brain capillaries and for metastatic outgrowth. Brain metastatic cells from lung cancer and breast cancer express high levels of anti-PA serpins, including neuroserpin and serpin B2, to prevent plasmin generation and its metastasis-suppressive effects. By protecting cancer cells from death signals and fostering vascular co-option, anti-PA serpins provide a unifying mechanism for the initiation of brain metastasis in lung and breast cancers.

INTRODUCTION

Metastasis is the main cause of death from cancer, but biologically, metastasis is a rather inefficient process. Most cancer cells that leave a solid tumor perish, and much of this attrition happens as circulating cancer cells infiltrate distant organs (Chambers et al., 2002). Although mechanisms for early steps of tumor cell dispersion and late stages of macrometastatic outgrowth are known (Valastyan and Weinberg, 2011; Vanharanta and Massagué, 2013), the factors that determine the survival and adaptation of disseminated cancer cells in vital organs remain obscure. Identifying these factors is particularly critical in the case of brain metastasis. Brain relapse is the most devastating complication of cancer, with acute neurologic distress and high mortality being typical traits (Gavrilovic and Posner, 2005). The incidence of brain metastasis is ten times higher than that of all primary brain tumors combined (Maher et al., 2009). Lung cancer and breast cancer are the top sources of brain metastasis, together accounting for nearly two-thirds of total cases. However, it is in the brain that infiltrating cancer cells face a particularly high rate of attrition, as shown in experimental models (Kienast et al., 2010). Brain metastasis tends to be a late complication of cancer in the clinic (Feld et al., 1984; Karrison et al., 1999) and is rare in mice with genetically engineered tumors that readily metastasize to other organs (Francia et al., 2011; Winslow et al., 2011).

The severe attrition of metastatic cells in the brain and the late occurrence of brain metastasis in the clinic argue that circulating cancer cells face major hurdles in colonizing this organ. Cancer cells require specialized mechanisms to traverse the blood-brain barrier (BBB), and molecular mediators of this process were recently identified (Bos et al., 2009; Li et al., 2013). However, most cancer cells that pass the BBB die (Heyn et al., 2006; Kienast et al., 2010). Interestingly, cancer cells that succeed in infiltrating the brain present the striking feature of adhering to the surface of capillaries and growing as a sheath around the vessels, whereas those that fail to co-opt the vasculature also fail to thrive (Carbonell et al., 2009; Kienast et al., 2010; Lorger and Felding-Habermann, 2010). What kills most cancer cells that pass through the BBB, and what enables the few survivors to co-opt the vasculature are questions of biologic and clinical interest.

Seeking to define common mechanisms for metastatic colonization of the brain, we focused on a small set of genes whose expression is associated with brain metastatic phenotypes in

both lung and breast adenocarcinoma models. One of these genes, *SERPINI1*, encoding the plasminogen activator (PA) inhibitor neuroserpin (NS), is normally expressed mainly in the brain. Tissue PA (tPA) and urokinase PA (uPA) convert plasminogen into plasmin, an endopeptidase that mediates fibrinolysis in blood clot resolution and is also involved in the stromal response to brain injury (Benarroch, 2007; Sofroniew and Vinters, 2010). Reactive astrocytes are major sources of PAs in ischemia and neurodegenerative injury (Adhami et al., 2008; Ganesh and Chintala, 2011; Teesalu et al., 2001). To avert the deleterious action of plasmin, neurons express NS (Yepes et al., 2000). We found that by secreting PA inhibitory serpins, brain metastatic cells thwart the lethal action of plasmin from the reactive stroma. Moreover, suppression of Fas-mediated cancer cell killing and promotion of L1 cell adhesion molecule (L1CAM)-mediated vascular co-option lie downstream of anti-PA serpin action as critical requirements for the initiation of brain metastasis.

RESULTS

Association of PA-Inhibitory Serpins with the Brain Metastatic Phenotype

To identify shared mediators of brain metastasis, we compared the transcriptomic signatures of brain metastatic subpopulations (BrM) that were isolated from the lymph-node-derived human lung adenocarcinoma cell lines H2030 and PC9 (Nguyen et al., 2009) and the pleural-effusion-derived breast cancer cell lines MDA-MB-231 (MDA231 for short) and CN34 (Bos et al., 2009; Figure 1A). Seven genes were upregulated in brain metastatic cells compared with the source parental lines in at least three of the four models (Figure S1A available online). Among these genes, *LEF1* was previously defined as a mediator of WNT signaling in brain metastasis (Nguyen et al., 2009). Of the remaining genes, only *SERPINI1*, encoding NS, was associated with brain relapse in human primary tumors (see below). This was intriguing because NS expression is normally restricted to neurons, where it protects against PA cytotoxicity (Yepes et al., 2000).

The 36 serpin family members in human collectively target 18 proteases (Irving et al., 2000). Four serpins (NS and serpins B2, E1, and E2) selectively inhibit PA (Law et al., 2006). The mRNA levels for three of the four were upregulated >3-fold in brain metastatic cells (Figure 1A). Only one other serpin, *SERPIND1*, was also upregulated (Figure 1A). Serpin D1 inhibits thrombin, which cooperates with plasminogen in cerebral injury (Fujimoto et al., 2008). Bone metastatic derivatives (MDA231-BoM) (Kang et al., 2003) and lung metastatic derivatives (MDA231-LM2) (Minn et al., 2005) were available for comparisons with MDA231-BrM2, and showed little or no upregulation of the serpins (Figure 1B).

Additionally, we established the cell line ErbB2-P from a mouse mammary tumor driven by a mutant *ErbB2* transgene (Muller et al., 1988) and then isolated a brain metastatic derivative (ErbB2-BrM2) by selection of ErbB2-P in congenic mice. ErbB2-BrM2 cells showed a strong upregulation of serpins B2 and D1 compared with ErbB2-P (Figure 1A). We also screened four cell lines derived from lymph node metastases of genetically engineered $Kras^{G12D};p53^{-/-}$ mouse lung adenocarcinomas (Winslow et al., 2011). All four lines were highly metastatic to visceral organs but ranged widely in brain metastatic activity (Figures 1C and S1B), and brain metastasis was associated with high expression of serpins I1, B2, E2, and/or D1 (Figures 1C and 1D).

The upregulation of NS and serpin B2 in brain metastatic cells was confirmed at the protein level (Figures S1C and S1D). Moreover, conditioned media from brain metastatic cells inhibited the generation of plasmin activity from plasminogen (Figures 1E, 1F, and S1E). The only exception was PC9-BrM3, a cell line that is less aggressive in brain metastasis compared with H2030-BrM3 (Nguyen et al., 2009) and lacks upregulated anti-PA serpins (Figures 1A, S1C, and S1D).

NS and Serpin B2 in Human Brain Metastasis Tissues

Focusing on the two most frequently upregulated anti-PA serpins in these models, NS and serpin B2, we queried gene-expression data from 106 primary lung adenocarcinomas with relapse annotation (Nguyen et al., 2009). The expression level of *SERPINI1* and *SERPINB2* in the tumors was associated with brain relapse, both as individual genes (data not shown) and combined ($p = 0.018$, hazard ratio = 2.33 ± 0.3; Figure 1G). Expression of the two genes was not significantly associated with metastasis to bone or lungs ($p = 0.89$, hazard ratio = 0.91 ± 0.33; $p = 0.36$, hazard ratio = 0.76 ± 0.27; Figures S1F and S1G). *SERPINI1* and *SERPINB2* expression in breast tumors was not a predictor of brain metastasis ($p = 0.21$, hazard ratio = 0.96 ± 0.16; Figure S1H), though in most of these cases brain relapse was a late event that might have been seeded from metastases in other organs.

We performed an immunohistochemical analysis of NS and serpin B2 in human brain metastasis tissue using mouse brain lesions formed by serpin-expressing human cancer cells as a reference (Figure S1I). Among 33 metastases of non-small-cell lung carcinomas (NSCLCs), 45% scored positive for NS and 94% scored positive for serpin B2. Among 123 metastases from various subtypes of breast cancer, 77% scored positive for NS and 34% scored positive for serpin B2 (Figures 1H, 1I, S1I, and S1J). The immunoreactivity was distributed diffusely in the cytoplasm of carcinoma cells and only minimally in the scant extracellular stroma. Positivity for NS and serpin B2 in the inflammatory infiltrate was limited.

Plasmin Is Lethal to Cancer Cells that Invade the Brain Parenchyma

The MDA231-BrM2 and H2030-BrM3 models are metastatic to the brain from orthotopic tumors and the arterial circulation (Bos et al., 2009; Nguyen et al., 2009). We inoculated these cells into the arterial circulation of immunodeficient mice via the left cardiac ventricle and fixed the tissue to count cancer cells lodged in the brain capillary network at different time points (Figures 2A–2C and S2A). One day after inoculation, we observed isolated cancer cells trapped within brain capillaries (Figure 2B, and H2030-BrM3 data not shown). Cells passing through the BBB were observed between days 2 and 7 after inoculation (Figures 2B and S2B). All cells that remained within capillaries on day 7 stained positive for the apoptosis marker, cleaved caspase-3 (Figures S2C and S2D). No intravascular cells were observed thereafter. In parental MDA231, the number of extravasated cells

A

Cell line	Species	Tumor type	Source	Serpin mRNA (relative level)			
				I1 (NS)	*B2*	*E2*	*D1*
H2030-BrM3	Human	Lung adenocarcinoma (*KRAS* mutant)	Lymph node	3.4	0.3	1.4	0.3
PC9-BrM3	Human	Lung adenocarcinoma (*EGFR* mutant)	Lymph node	1.2	0.7	0.8	2.8
MDA231-BrM2	Human	TN breast carcinoma (ER-, PR-, HER2-)	Pleural fluid	5.0	10.1	0.5	5.1
CN34-BrM2	Human	TN breast carcinoma (ER-, PR-, HER2-)	Pleural fluid	8.9	15.5	9.6	8.5
Kras/p53-482N1	Mouse	Lung adenocarcinoma (*Kras* mutant, *p53* null)	Lymph node	4.3	2.9	37.6	62.2
ErbB2-BrM2	Mouse	Breast carcinoma (*ErbB2* hyperactive)	Mammary tumor	0.5	15.7	1.9	7.0

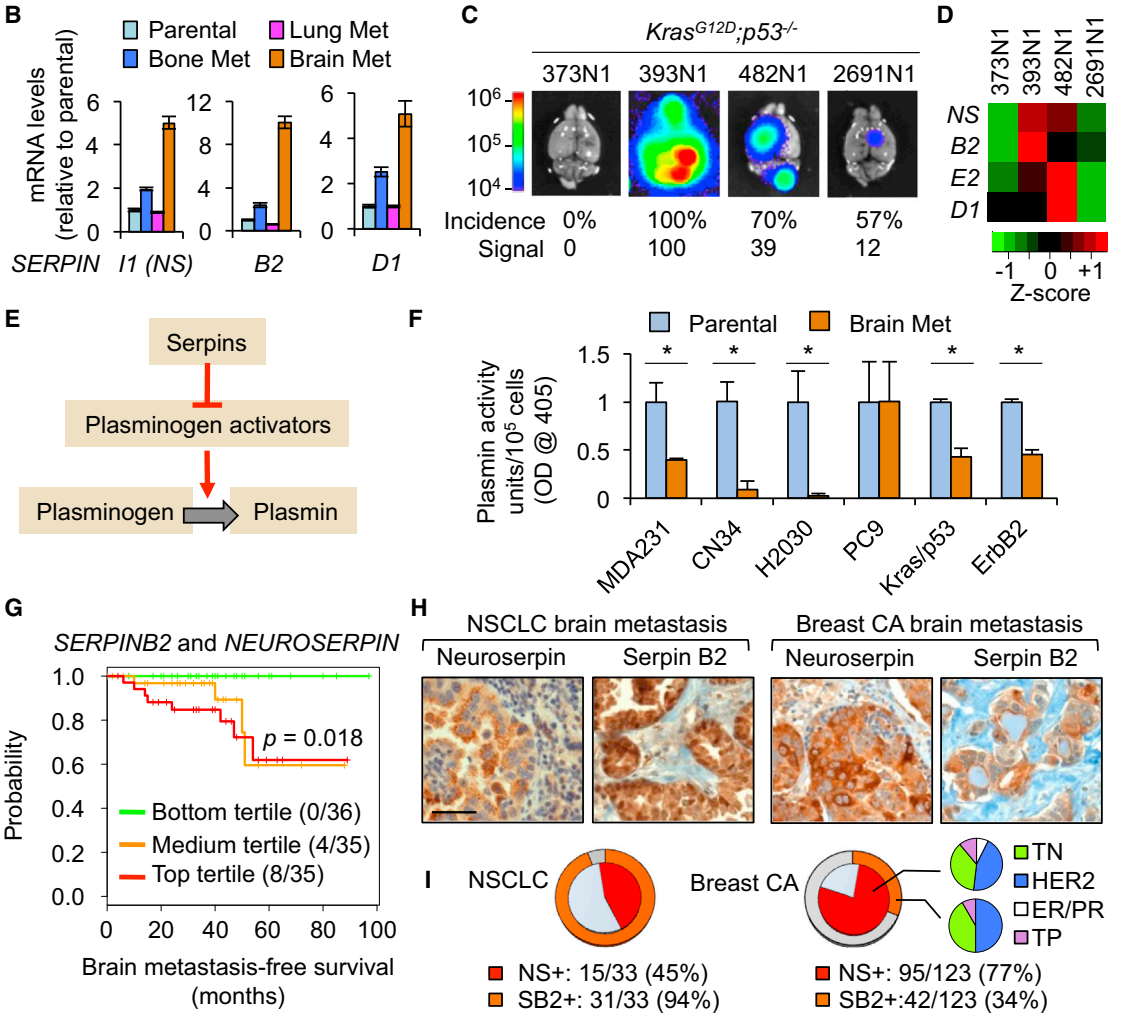

Figure 1. Association of PA-Inhibitory Serpins with the Brain Metastatic Phenotype

(A) Serpin mRNA levels in brain metastatic cell lines relative to the levels in counterparts not metastatic to brain. TN, triple negative; ER−, estrogen receptor negative; PR−, progesterone receptor negative.

(B) mRNA levels of the indicated serpins in the parental MDA231 cell line and derivatives with different metastatic tropisms. Error bars, 95% confidence interval.

(C) Representative ex vivo bioluminescence images of brains from syngeneic mice inoculated with *Kras*^{G12D};*p53*$^{-/-}$ mouse lung cancer cell lines. The percentage of mice that developed brain metastasis and the mean BLI photon flux signal are indicated. n = 10.

(D) Heatmap of serpin mRNA expression in *Kras*^{G12D};*p53*$^{-/-}$ derivatives.

(legend continued on next page)

dropped sharply after day 5 and rarely recovered (Figure S2B). In line with previous reports (Kienast et al., 2010; Lorger and Felding-Habermann, 2010), >90% of cancer cells that entered the brain disappeared within days. In MDA231-BrM2, the number of extravasated cells increased until day 7 and then dropped sharply by day 10, but recovered by day 16. The survivors were bound to and stretched over the abluminal surface of brain capillaries (Figures 2A and 2B). Outgrowth occurred mainly on co-opted vessels (Figure 2C; summarized in Figure 2D).

In the brain, metastatic cells were in close proximity to astrocytes (Figures 2E, S2E, and S2F), microglia, and neurons (Figures S2G–S2J). Reactive astrocytes, identified by high glial fibrillary acidic protein (GFAP) expression and a stellate morphology, were associated with cancer cells right after extravasation and thereafter (Figures 2E, S2E, and S2F). Reactive astrocytes are a major source of PA in brain injury (Adhami et al., 2008; Ganesh and Chintala, 2011). Indeed, mouse brain sections harboring metastatic cells showed tPA and uPA immunoreactivity associated with astrocytes (Figures 2F and 2G). Mouse astrocytes cultures were superior to microglia for converting plasminogen to plasmin (Figure S2K). Neurons produce plasminogen for neurite and synapse formation (Gutiérrez-Fernández et al., 2009). Plasminogen immunoreactivity was associated with NeuN+ neurons near metastatic cells in mouse brain (Figure 2H). Thus, the brain metastasis microenvironment contains the necessary components for plasmin production.

To determine whether plasmin is harmful to metastatic cells in the brain parenchyma, we used mouse brain slice cultures (Figure 2I). When placed on top of brain slices, H2030-BrM3 cells migrated into the tissue, targeted blood capillaries, and spread on the surface of the vessels (Figure 2J). H2030-BrM3 cells proliferated under these conditions (Figures 2K and 2L), whereas parental H2030 did not proliferate (Figures 2K and 2L) and underwent apoptosis (Figures 2M and 2N). Similar results were obtained with MDA231 cells (Figure S2N). In cocultures of cancer cells with astrocytes and microglia, plasminogen addition triggered apoptosis in parental H2030, but not in H2030-BrM3 (Figures S2L and S2M). The brain slices contained endogenous plasmin activity, and addition of a plasmin inhibitor, α2-antiplasmin (Bajou et al., 2008), inhibited this activity (Figures S2O and S2P) and increased the survival of parental H2030 cells in the slices (Figures 2K–2N). Of note, addition of plasmin to cancer cell monolayer cultures did not trigger apoptosis (Figure S2Q). These results suggested that plasmin acting through unknown substrates kills infiltrating cancer cells in the brain, whereas highly metastatic cells are shielded from this threat (Figure 2O).

NS Protects Metastatic Cells from Plasmin-Mediated Attrition

To investigate the role of NS in brain metastasis, we first used the H2030-BrM3 model, in which only this serpin is upregulated (refer to Figure 1A). Brain lesions formed by H2030-BrM3 cells showed strong NS immunoreactivity (Figure S3A). Two small hairpin RNAs (shRNAs) that decreased NS expression and secretion by >85% (Figures S3B and S3C) did not affect the growth of H2030-BrM3 cells in culture (Figure S3D) but inhibited the metastatic activity of these cells, as shown by bioluminescence imaging (BLI) of marker luciferase in vivo (Figures 3A–3D), BLI ex vivo (Figure 3B), and marker GFP expression in brain sections (Figure 3E). NS depletion in H2030-BrM3 decreased the number and size of brain lesions (Figures 3F and S3E), with a >90% overall reduction in brain tumor burden (Figure 3G). The few macroscopic lesions that developed were rich in NS (Figure S3F), suggesting escape from the knockdown.

NS knockdown did not inhibit the entry of H2030-BrM3 cells into the brain parenchyma (Figure S3G) or their ability to cross an endothelial/astrocyte BBB-like barrier in vitro, whereas the knockdown of *ST6GalNaC5*, a mediator of BBB extravasation, did (Bos et al., 2009; Figures S3H and S3I). In brain slice assays, NS knockdown in H2030-BrM3 cells decreased the number of infiltrated cells (Figures 3H and 3I) and increased apoptosis (Figures 3H and 3J), whereas overexpression of NS in parental H2030 and MDA231 cells had the opposite effects (Figures 3K and 3L).

Brain Metastasis Mediated by the PA Inhibitory Function of NS

PC9-BrM3 can infiltrate the brain but are less aggressive than H2030-BrM3 in colonizing it (Nguyen et al., 2009) and show no upregulation of anti-PA serpins (refer to Figure 1A). PC9-BrM3 cells were stably transduced with vectors encoding the wild-type NS or a mutant (NSΔloop) that is devoid of PA inhibitory function (Takehara et al., 2009; Figures S3J–S3M). Wild-type NS significantly increased the brain metastatic activity of PC9-BrM3, whereas the mutant did not (Figures 3M and 3N). PC9-BrM3 cells are also metastatic to bone (Nguyen et al., 2009), and NS overexpression did not markedly affect this activity (Figures 3M and 3N). $NS^{\Delta loop}$ was also ineffective at protecting the parental H2030 and MDA231 cells from apoptosis in brain tissue (Figures 3K and 3L). These results suggest that NS mediates brain metastatic activity in cancer cells by inhibiting PA.

(E) Summary of the serpin-PA-plasmin cascade.
(F) Inhibition of plasminogen conversion into plasmin by cell culture supernatants of the indicated cell lines. Plasmin activity was determined by a chromogenic assay. Data are averages ± SEM from triplicate experiments.
(G) Kaplan-Meier analysis of brain-metastasis-free survival in 106 cases of lung adenocarcinoma classified based on *SERPINB2* and *SERPINI1* mRNA levels in the primary tumor. The p value was calculated from a Cox proportional hazard model, with *SERPINB2* and *SERPINI1* expression treated as a continuous variable.
(H) Representative human brain metastasis samples from lung and breast cancer stained with antibodies against NS or serpin B2.
(I) Proportion of metastasis samples that scored positive for NS immunostaining (red) or serpin B2 immunostaining (orange) in 33 cases of NSCLC and 123 cases of breast carcinoma. Small diagrams in the breast cancer set represent the primary tumor subtype (HER2, HER2+; ER/PR, hormone-receptor positive; TP, triple positive) of the serpin-positive samples for which this information was available. Brain metastases that scored positive for both serpins comprised 42% and 34% of the lung cancer and breast cancer cases, respectively. Samples scored as positive had >80% of neoplastic cells showing positive reactivity.
Scale bar, 100 μm. See also Figure S1.

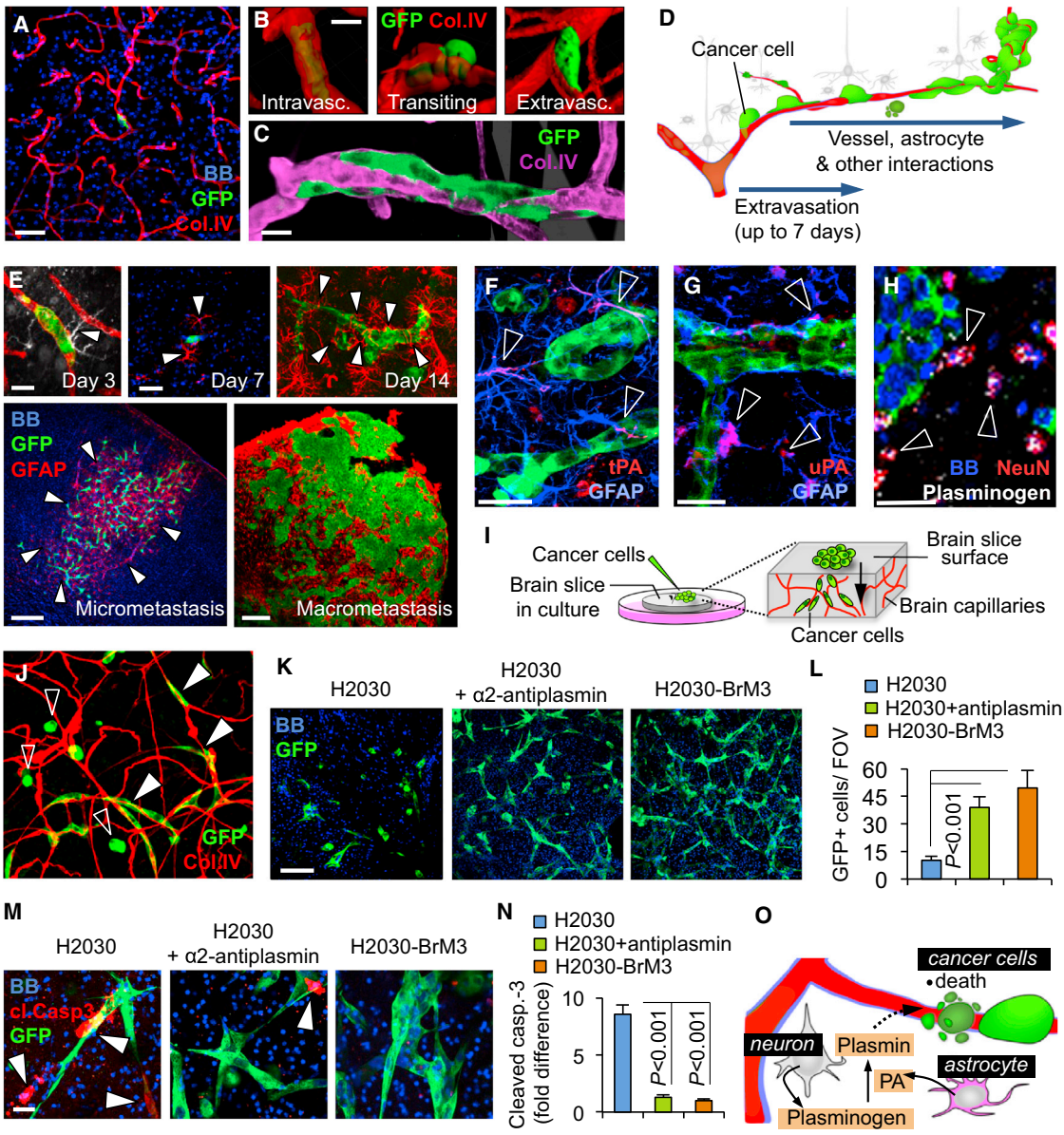

Figure 2. Vascular Co-Option, Outgrowth, and Escape from Stromal Plasmin Action

(A) Metastatic cell interactions with brain capillaries. MDA231-BrM2 cells (green) remain bound to brain capillaries (red) after completing extravasation.

(B) Confocal analysis of the extravasation steps showing a GFP+ MDA231-BrM2 cell.

(C) Cluster of extravasated MDA231-BrM2 cells forming a sheath around a brain capillary. All extravasated cells initially grew in this manner. Blue, nuclear staining.

(D) Schema representing the initial steps and interactions during metastatic colonization of the brain.

(E) Exposure of metastatic H2030-BrM3 cells to GFAP+ reactive astrocytes (arrowheads) in the brain parenchyma at different time points after inoculation of cancer cells into the circulation. Day 3: red, collagen IV; white, GFAP; green, GFP+ cancer cells; blue, nuclear staining.

(F and G) tPA and uPA immunofluorescence staining (arrowheads) associated with GFAP+ astrocytes in a mouse brain harboring GFP+ H2030-BrM3 cells (green).

(H) Plasminogen immunofluorescence staining (white, arrowheads) is associated with NeuN+ neuron bodies (red) near a cluster of GFP+ metastatic cells (green) in a mouse brain. Blue, nuclei.

(I) Schema of brain slice organotypic cultures. Cancer cells placed on the surface of slices migrate into the tissue and seek microcapillaries.

(J) Representative image of a brain slice harboring infiltrated H2030-BrM3 cells that are still round (open arrowheads) or already spread over brain capillaries (closed arrowheads).

(K) Representative confocal images of brain slice tissue infiltrated with the indicated cancer cells. α2-antiplasmin was added to the indicated cultures. Note the lower density and disorganized aspect of parental cells compared with the stretched morphology of BrM3 cells or parental cells with α2-antiplasmin.

(L) Quantification of GFP+ cancer cells in the experiments of (K). The numbers of cells per field of view (FOV) are averages ± SEM, n = 6–10 brain slices, scoring at least two fields per slice, in at least two independent experiments.

(legend continued on next page)

Role of Anti-PA Serpins in Brain Metastatic Breast Cancer Cells

Unlike the H2030-BrM3 cells, most other brain metastatic models and a large proportion of human brain metastatic tissues overexpressed not one but multiple anti-PA serpins (refer to Figures 1A and 1I). In MDA231-BrM2, a triple knockdown of the three upregulated serpins (B2, D1, and NS; Figures S4A–S4C) inhibited the brain metastatic activity of the cells more than did the knockdown of any individual serpin (Figures 4A, 4B, S4G, and S4H). The knockdown of serpin B2 (Figures S4D and S4E) partially inhibited the brain metastatic activity of MDA231-BrM2, and the lost activity could be rescued by enforced overexpression of NS (Figures 4A, 4B, and S4F). Clonal cell lines isolated from the MDA231-BrM2 population showed heterogeneity in the overexpression of anti-PA serpins. Compared with the parental MDA231 population, we observed upregulation of NS in nine out of ten clones, serpin B2 in five out of ten, and serpin D1 in eight out of ten (Figures 4C and S4I). As a trend, clones with high levels of the three serpins were more metastatic to brain than were clones with lower levels (Figures 4D and S4J). Clones with high levels of NS and serpin D1 lost brain metastatic activity when transduced with *NS* shRNA (Figure 4E). In the ErbB2-BrM2 model, the knockdown of its only upregulated anti-PA serpin, serpin B2 (refer to Figure 1A), strongly decreased the brain metastatic activity in immunocompetent mice (Figures 4F–4H). In sum, the evidence indicated that expression of one or more anti-PA serpins provides lung cancer and breast cancer cells with a critical advantage in the formation of brain metastases.

Metastatic Cells Face FasL in the Brain

We searched plasmin substrate databases (MEROPS and CutDB) for proteins whose cleavage might affect brain metastasis (Bajou et al., 2008; Chen and Strickland, 1997; Nayeem et al., 1999; Pang et al., 2004). We focused first on FasL, a pro-apoptotic cytokine. FasL is a membrane-anchored homotrimeric protein that binds to Fas, a receptor that activates proapoptotic caspases through the adaptor protein FADD (Ashkenazi and Dixit, 1998). FasL is highly expressed in reactive astrocytes in ischemia, brain trauma, Alzheimer's disease, encephalomyelitis, and multiple sclerosis (Choi and Benveniste, 2004). Astrocytes are the main source of FasL against invading T cells in encephalomyelitis (Wang et al., 2013). Plasmin cleaves FasL at Arg144, releasing sFasL as a diffusible cell death signal (Bajou et al., 2008; Fang et al., 2012). Therefore, we asked whether anti-PA serpins shield cancer cells from the lethal action of plasmin-mobilized sFasL (Figure 5A).

FasL immunoreactivity in brain sections harboring H2030-BrM3 lesions was concentrated on reactive astrocytes (Figures 5B and S5A). Human and mouse astrocytes expressed FasL in culture (Figures 5C and S5B). Addition of plasminogen decreased the level of cell-bound FasL in these cultures and increased sFasL in the supernatants (Figures 5C, 5D, and S5C–S5E). Addition of anti-PA serpins or antiplasmin decreased the level of sFasL in mouse brain slices (Figure 5E). These results showed that the PA-plasmin system can mobilize stromal FasL in response to metastatic invasion of the brain.

H2030, PC9, MDA231, and CN34 expressed Fas, as did their BrM derivatives (Figure S5F). Addition of sFasL caused apoptosis in BrM cells in monolayer cultures (Figures S5G–S5I) and in brain tissue (Figures 5F–5H), even in the presence of α2-antiplasmin (Figure S5J). Conversely, addition of anti-FasL blocking antibody protected parental H2030 cells against apoptosis in brain tissue (Figures 5G–5I). Thus, brain metastatic cells are susceptible to apoptosis if they are exposed to sFasL in the brain parenchyma, and this occurs downstream of plasmin.

NS Shields Brain Metastatic Cells from Fas-Mediated Killing

To determine whether Fas signaling caused the death of cancer cells that infiltrated the brain, we used a FADD truncation mutant that lacks the death effector domain (FADD-DD construct) and acts as a dominant-negative inhibitor of Fas signaling (Chinnaiyan et al., 1996; Figure 5J). Transduction of FADD-DD in the H2030-BrM3 cell line (Figure 5K) prevented the activation of caspase 3 by sFasL (Figure 5L). The apoptosis that anti-PA serpin-depleted BrM cells suffer in brain tissue (refer to Figures 3H–3J and S5L) could be prevented by adding anti-FasL blocking antibodies to the tissue cultures, as well as by enforcing the expression of FADD-DD in the cancer cells (Figures 5M, 5N, and S5L). Moreover, FADD-DD partially rescued the metastatic activity of NS-depleted H2030-BrM3 (Figure 5O). Collectively, these results showed that anti-PA serpin activity shields metastatic cells from FasL attack in the brain.

The Plasmin Target L1CAM Mediates Cancer Cell Adhesion

Although inhibition of Fas signaling with FADD-DD protected NS-depleted cancer cells from death in the brain, it did not fully restore their metastatic activity (Figure 5O). The NS-depleted, FADD-DD-expressing H2030-BrM3 cells formed smaller lesions that were less well organized (Figure S6A). Therefore, we postulated that anti-PA serpins promote brain metastasis by doing more than just preventing FasL action.

Several clues led us to consider L1CAM as a relevant mediator of metastasis in this context. L1CAM is mainly expressed in neural tissues and in tumors (Schäfer and Altevogt, 2010). It consists of six immunoglobulin-like (Ig) domains, five fibronectin-like (FN) domains, a transmembrane region, and

(M) Cleaved caspase-3 immunofluorescence staining in brain slices harboring the indicated cells and additions.

(N) Quantification of cleaved caspase-3-positive cancer cells in the experiments of (M). Values are quantified as (L), normalized to H2030-BrM3, and are averages ± SEM.

(O) Schematic summary showing neurons and astrocytes as sources of plasminogen and PA, respectively, and the lethal effect of the resulting plasmin on infiltrating cancer cells.

All p values by Student's t test. Scale bars, 25 μm (A), 5 μm (B and C), 5 μm (day 3), 15 μm (day 7), 25 μm (day 14), 70 μm (micrometastasis), 100 μm (macrometastasis) (D), 10 μm (F–H), 100 μm (K), and 5 μm (M). See also Figure S2.

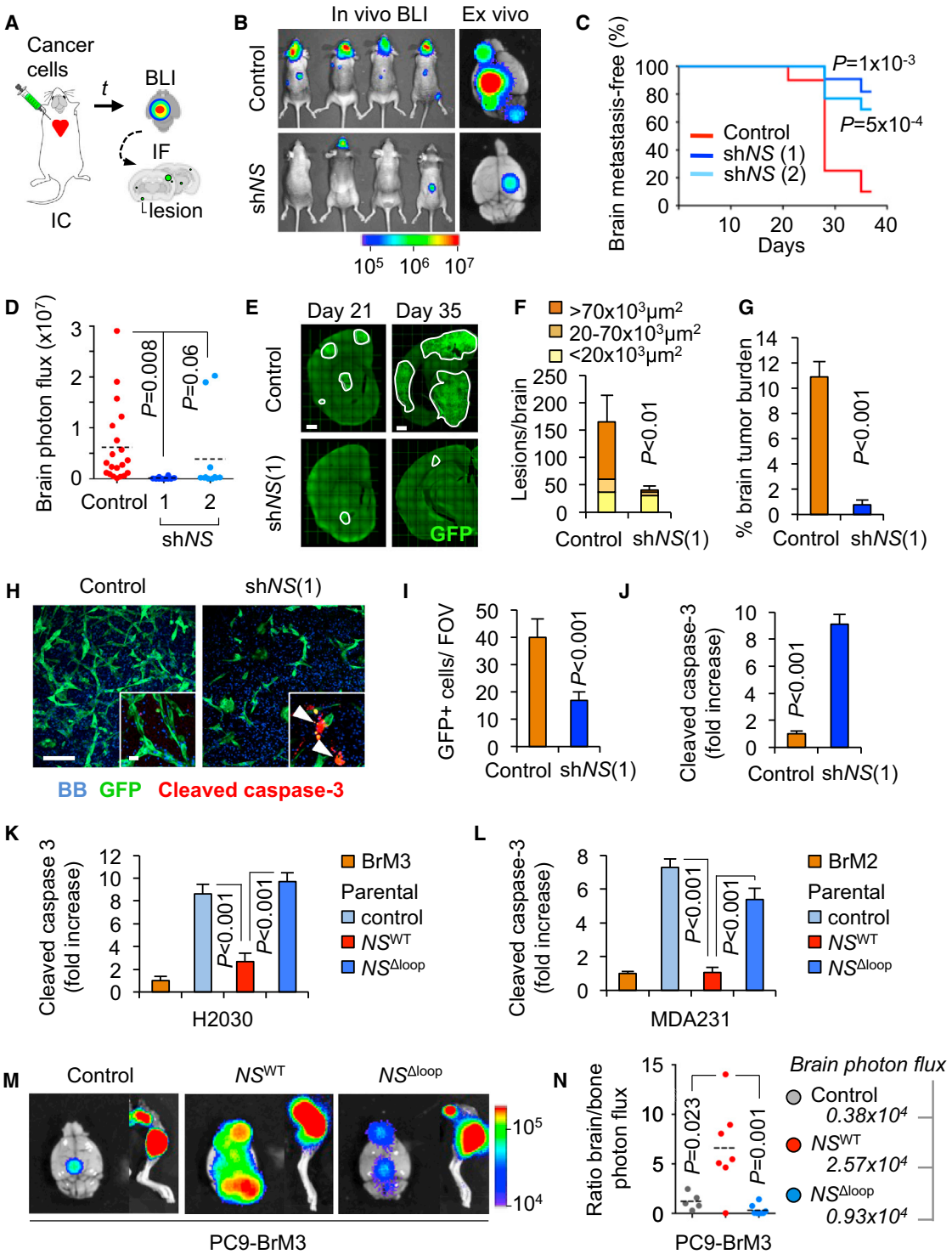

Figure 3. NS Mediates Brain Metastasis

(A) Schema of the experimental design.

(B) Representative images of whole-body BLI and brain ex vivo BLI 5 weeks after inoculation of H2030-BrM3 cells transduced with control shRNA or *NS* shRNA (sh*NS*).

(C) Kaplan-Meier plot of brain-metastasis-free survival in the experiment of (B). Control (n = 20) and two different sh*NS* (sh*NS* (1), n = 11; sh*NS* (2), n = 13) were analyzed; p values were obtained with the log rank Mantel-Cox test.

(D) Quantification of ex vivo BLI in brains from (B).

(legend continued on next page)

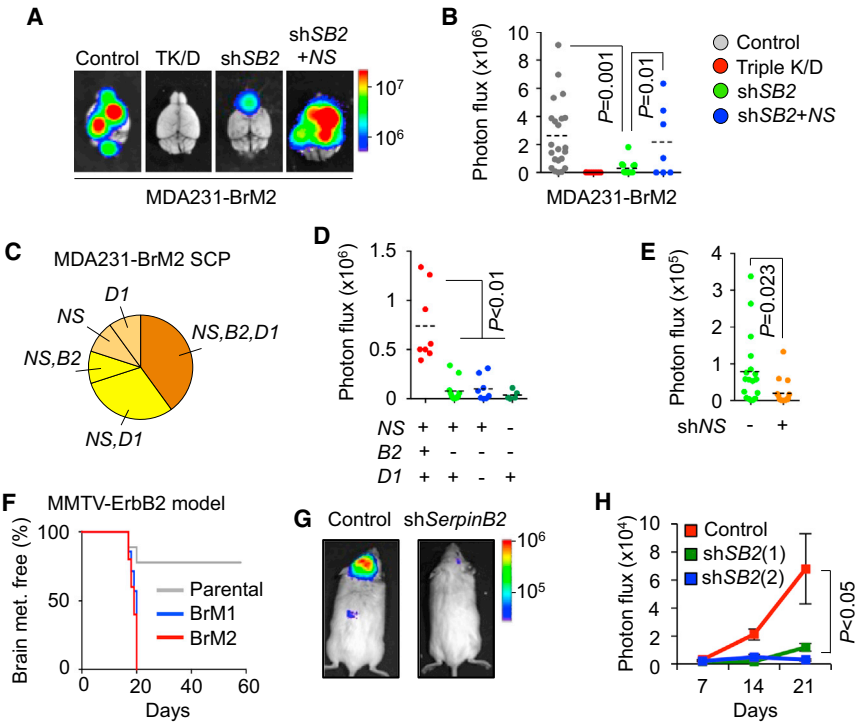

Figure 4. Anti-PA Serpins Mediate Brain Metastasis by Breast Cancer Cells

(A and B) MDA231-BrM2 cells transduced with control vector; shRNA vectors targeting *NS*, *SERPINB2*, and *SERPIND1* (triple K/D); *SERPINB2* shRNA (sh*SB2*); or sh*SB2* plus an NS-expressing vector were inoculated into the arterial circulation of immunodeficient mice. Brain metastasis burden was visualized by ex vivo brain BLI (A) and quantitated (B). Control n = 22, triple K/D n = 9, sh*SB2* n = 14, sh*SB2* and NS n = 8.

(C) Distribution of clones (single-cell progenies [SCPs]) overexpressing one, two, or three of the indicated serpins among ten clonal cell lines isolated from the MDA231-BrM2 population.

(D) Ex vivo brain BLI quantification from different MDA231-BrM2 SCPs injected. Red dots, SCP (high levels of all serpins), n = 8; light green dots, SCP (low levels of serpin B2), n = 11; blue dots, SCP (low levels of serpin B2 and D1), n = 8; dark green dots, SCP (low levels of serpin B2 and NS), n = 5. The p value was determined by Student's t test.

(E) SCPs with high levels of NS and serpin D1 were subjected to *NS* knockdown and tested for brain metastatic activity.

(F) Kaplan-Meier survival curves for brain-metastasis-free survival in syngeneic mice inoculated with parental ErbB2-P cells (n = 9) or brain metastatic derivatives ErbB2-BrM1 (n = 7) and ErbB2-BrM2 (n = 5). Survival curves were compared using the log rank Mantel-Cox test. ErbB2-P versus ErbB2-BrM1, p = 0.0045; ErbB2-P versus ErbB2-BrM2, p = 0.0053.

(G and H) Representative images (G) and quantification (H) of brain metastasis BLI photon flux formed by ErbB2-BrM2 or these cells expressing two different serpin *B2* shRNAs (sh*SB2*). Control, n = 10; sh*SB2* (1), n = 10; sh*SB2* (2), n = 6.

Data are averages ± SEM. All p values were determined by Student's t test, except in (F). See also Figure S4.

an intracellular domain (Figure 6A). The L1CAM Ig-like repeats mediate homo- and heterophilic interactions for axon guidance (Maness and Schachner, 2007). L1CAM binds to itself, to integrins (Felding-Habermann et al., 1997), and to other proteins (Castellani et al., 2002; Donier et al., 2012; Kulahin et al., 2008). L1CAM expression in tumors is implicated in invasion (Voura et al., 2001) and associated with poor prognosis (Doberstein et al., 2011; Schröder et al., 2009). Plasmin cleaves L1CAM at dibasic motifs (Lys860/Lys863), disrupting the capacity for cell adhesion (Nayeem et al., 1999; Silletti et al., 2000; Figure 6A).

Hence, we postulated that L1CAM mediates plasmin-sensitive vascular co-option by metastatic cells in the brain. L1CAM was expressed in the cancer cell lines regardless of their metastatic activity, tumor type, or species of origin (Figures S6B and S6C). H2030-BrM3 cells readily adhered to monolayers of human brain microvascular endothelial cells (HBMECs; Figures 6B and 6C) and to monolayers of their own (Figure 6D). RNAi-mediated knockdown of L1CAM (Figure S6B) inhibited these cell-cell binding activities (Figures 6C and 6D). Addition of plasmin to cancer cell monolayers caused a decrease in cell-associated L1CAM levels, as shown by flow cytometry (Figure 6E) and by the accumulation of a 150 kDa fragment in the media (Figure 6F; Mechtersheimer et al., 2001). Moreover, plasmin-treated H2030-BrM3 cells lost cell adhesion capacity (Figures 6G and 6H).

(E) Representative images of coronal brain sections analyzed with immunofluorescence (IF) against GFP at 21 or 35 days after inoculation of H2030-BrM3 cells into mice. Lesion contours are marked.

(F) Quantification of brain lesions according to size at the 21 day time point in (E). Control n = 5, sh*NS* n = 6 brains; p value refers to size distribution. For the total number of lesions, $p < 0.05$.

(G) Quantification of brain tumor burden in the experiment of (E). Control n = 5, sh*NS* n = 6.

(H) Representative images of control and *NS*-depleted H2030-BrM3 cells in brain slice assays. Insets show cleaved caspase-3 IF.

(I and J) Quantification of GFP+ cells (I) and cleaved caspase-3 (J) in the experiment of (H). Data are averages ± SEM; n = 6–10 slices, scoring at least two fields per slice, in at least two independent experiments.

(K and L) Quantification of cells that were positive for cleaved caspase-3, comparing parental and BrM cell lines, and the effect of overexpressing NS wild-type (NS^{WT}) or a mutant form unable to target PA ($NS^{\Delta loop}$) in parental cell lines H2030 (K) and MDA231 (L). Data are averages ± SEM, quantified as (J).

(M) Representative ex vivo BLI images of brains and hindlimbs from mice 21 days after inoculation with PC9-BrM3. Cells were transduced with empty vector (n = 5), NS^{WT} (n = 7), or $NS^{\Delta loop}$ mutant (n = 8).

(N) Ratio of photon flux in brain versus bone in the experiment of (M). Ex vivo brain mean BLI values are also shown.

All p values were calculated by Student's t test, except in (C). Scale bars, 250 μm (E), 100 μm, and 5 μm (inset) (H). See also Figure S3.

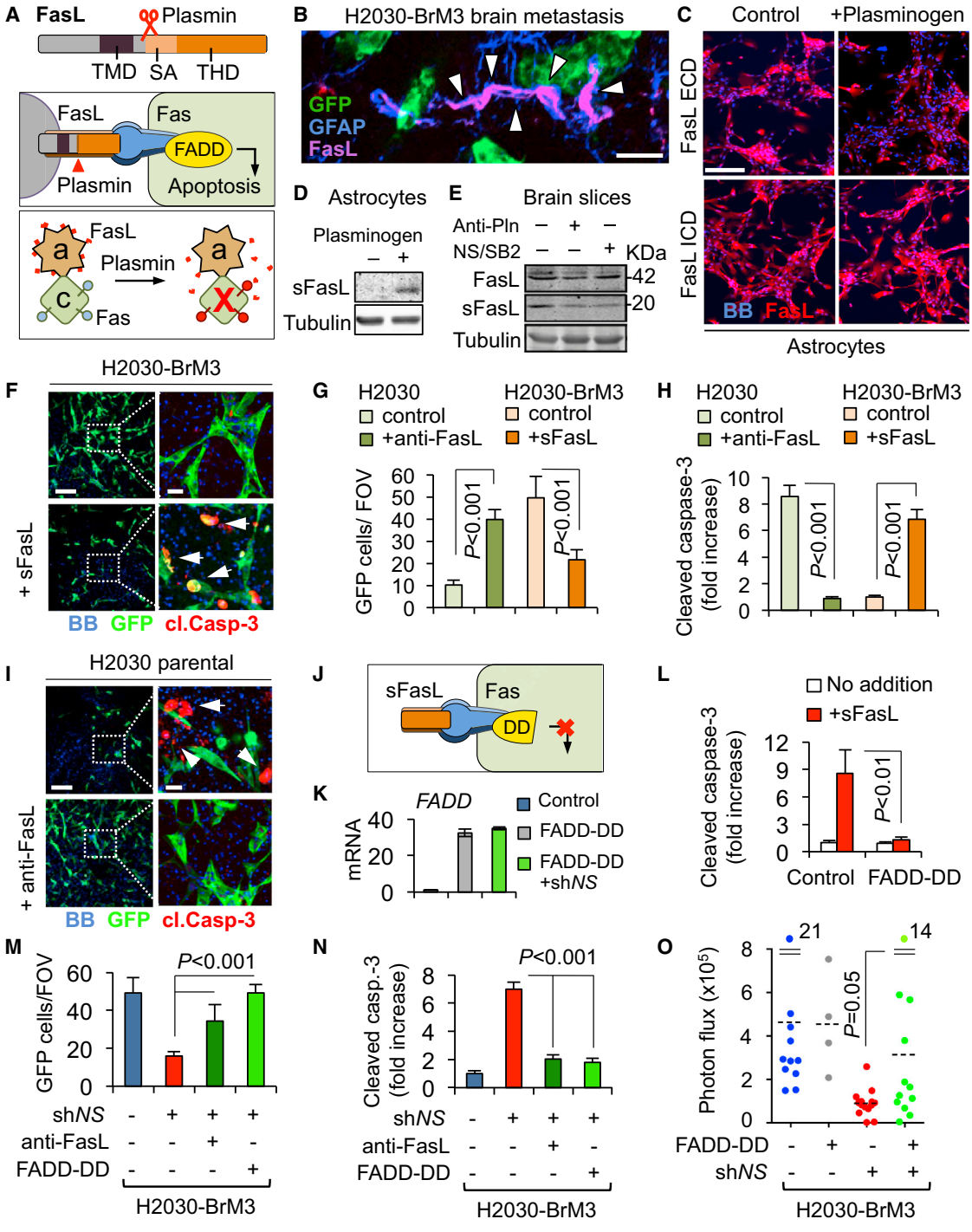

Figure 5. NS Shields Cancer Cells from FasL Death Signals

(A) Schema of FasL and its conversion by plasmin into sFasL, a diffusible trigger of apoptosis through Fas-FADD signaling. TMD, transmembrane domain; SA, trimeric self-assembly domain; THD, tumor necrosis factor-homology domain; red crosses, apoptotic cells; a, astrocyte; c, cancer cell.

(B) IF with antibodies against GFP (cancer cells), GFAP (reactive astrocytes), and FasL in a mouse brain harboring metastatic cells 21 days after arterial inoculation of H2030-BrM3.

(C) Images of astrocyte cultures incubated with exogenous plasminogen (1 μM) or no additions. Staining was performed with antibodies against the extracellular domain (ECD) or intracellular domain (ICD) of FasL.

(D) Western immunoblotting of supernatants from cultures shown in (C) using anti-FasL ECD antibodies.

(E) Mouse brain slices were incubated with α2-antiplasmin, NS, and serpin B2, or no additions. sFasL in tissue lysates was detected by western immunoblotting with anti-FasL ECD. Quantification of band density relative to tubulin (left to right) yielded sFasL:FasL ratios of 1, 0.51, and 0.28.

(legend continued on next page)

L1CAM Mediates Vascular Co-Option and Metastatic Outgrowth

The molecular basis for vascular co-option in cancer remains unknown. To address this issue, we asked whether L1CAM participates in vascular co-option by metastatic cells in the brain. L1CAM depletion in H2030-BrM3 cells did not affect their ability to grow in culture (Figure S6D), infiltrate brain tissue, or seek capillaries (Figures 6I and S6E). Notably, L1CAM depletion significantly reduced the ability of H2030-BrM3 and MDA231-BrM2 cells to spread on the abluminal surface of the capillaries (Figures 6I, 6J, and S6G). This was accompanied with a marked decrease in the proliferation marker Ki67 in vessel-associated cancer cells (Figure 6K), without changes in apoptosis markers (Figure S6F).

PC9-BrM3 cells, which do not overexpress endogenous anti-PA serpins, had a limited ability to spread on brain capillaries (Figures 6L and 6M). Enforced expression of NS in these cells not only augmented their metastatic activity (see Figure 3N) but also increased their spreading on brain capillaries (Figures 6L and 6M) and their proliferation on the co-opted vessels (Figure 6N). L1CAM depletion in PC9-BrM3-NS cells (Figures S6H and S6I) abrogated these NS-dependent gains (Figures 6L–6N).

L1CAM Supports Metastasis Initiation Downstream of NS

L1CAM immunostaining was clearly detectable on carcinoma cells in a majority of the human NSCLC brain metastasis samples examined, and tended to be concentrated at cell interfaces (Figures S7A and S7B). L1CAM-positive cells were present in clusters. In the brain of inoculated mice, extravasated H2030-BrM3 cells were spread over the basal lamina of capillaries, without discernible contacts with the endothelial cells (Figure 7A). L1CAM immunostaining in micrometastases was concentrated at the interfaces of cancer cells with capillaries and adjacent cancer cells (Figure 7B). In recently extravasated H2030-BrM3 cells, L1CAM-depletion allowed cell contact with capillaries but prevented cell spreading over the capillaries (Figure 7C). Twenty-one days later, L1CAM-depleted cells remained mostly as single cells or small clusters, whereas the wild-type cells readily expanded over the capillary network and formed large colonies (Figures 7D and 7E). L1CAM knockdown markedly decreased the overall brain metastatic activity of H2030-BrM3 and MDA231-BrM2 cells (Figures 7F–7H). Moreover, L1CAM depletion abrogated the gain in metastatic activity of PC9-BrM3 cells imparted by enforced NS overexpression (Figure 7I). These results argued that L1CAM expression in metastatic cells acts downstream of NS to mediate co-option of brain capillaries and metastatic outgrowth.

DISCUSSION

The growing incidence of brain metastasis warrants a better understanding of the molecular mechanisms that underlie this condition. Our findings illuminate two critical requisites for metastatic colonization of the brain, namely, the escape of infiltrating cancer cells from killing by reactive stromal signals, and the striking ability of the surviving cancer cells to co-opt brain capillaries for metastatic expansion. We show that a stromal PA-plasmin pathway and its inhibition by carcinoma serpins control both of these processes in brain metastasis from lung and breast cancers, suggesting a unified mechanism for metastatic colonization of the brain.

Anti-PA Serpins as Common Mediators of Brain Metastasis

Brain metastasis involves close and sustained interactions of cancer cells with brain capillaries and reactive astrocytes. Previous work (Carbonell et al., 2009; Kienast et al., 2010; Lorger and Felding-Habermann, 2010) and our own studies show that circulating cancer cells interact with capillary walls not only during extravasation but also thereafter, by attaching to the abluminal surface and growing as a sheath along the co-opted vessels. Cancer cells that infiltrate the brain are immediately exposed to astrocytes that abound in the perivascular space and produce deleterious signals to repel invading cells. Cancer cells must be shielded from such signals in order to survive and to extract benefits from the stroma, including benefits from astrocytes (Lin et al., 2010; Seike et al., 2011). We show that the expression of anti-PA serpins in cancer cells provides such a shield. Serpin D1 and three out of four known anti-PA serpins are expressed in our six brain metastasis models. The most prominent of these serpins, NS and B2, are expressed in a majority of brain metastases from lung cancer and breast cancer patients. The PA-plasmin system is well characterized in connection with its role in blood clot resolution, but its role in cancer has remained paradoxical. Although

(F) GFP+ H2030-BrM3 cells (green) were allowed to infiltrate brain slices in media containing added sFasL or no additions and scored for cleaved caspase-3 (red, inset).
(G and H) Quantification of total GFP+ cells (G) and apoptotic GFP+ cells (H) in the experiments of (F) (orange bars) and (I) (green bars). Data are averages ± SEM, n = 6–10 slices, scoring at least two fields per slice, from at least two independent experiments.
(I) GFP+ H2030 cells (green) were allowed to infiltrate brain slices in media containing anti-FasL blocking antibody or no additions. Anti-FasL prevented endogenous signals from triggering caspase-3 activation (red, inset).
(J) Depiction of FADD-DD overexpression (yellow shape) to suppress proapoptotic Fas signaling in cancer cells.
(K) *FADD* expression in H2030-BrM3 transduced with a FADD-DD vector.
(L) Quantification of apoptotic cells following sFasL addition to H2030-BrM3 cells transduced with the indicated vectors.
(M and N) Quantification of total GFP+ cells (M) and apoptotic GFP+ cells (N) in brain slices harboring the indicated GFP+ H2030-BrM3 transfectants and/or additions. Data are averages ± SEM and quantitated as (G) and (H).
(O) Brain metastatic activity of H2030-BrM3 cells transduced with the indicated vectors and inoculated into the arterial circulation of mice. BLI photon flux was quantitated in cells transduced with control shRNA (n = 11), FADD-DD (n = 4), *NS* shRNA (n = 14), or *NS* shRNA and FADD-DD (n = 12).
All p values were determined by Student's t test. Scale bars, 25 μm (B), 200 μm (C), 100 μm (F and I), and 5 μm (insets in F and I).
See also Figure S5.

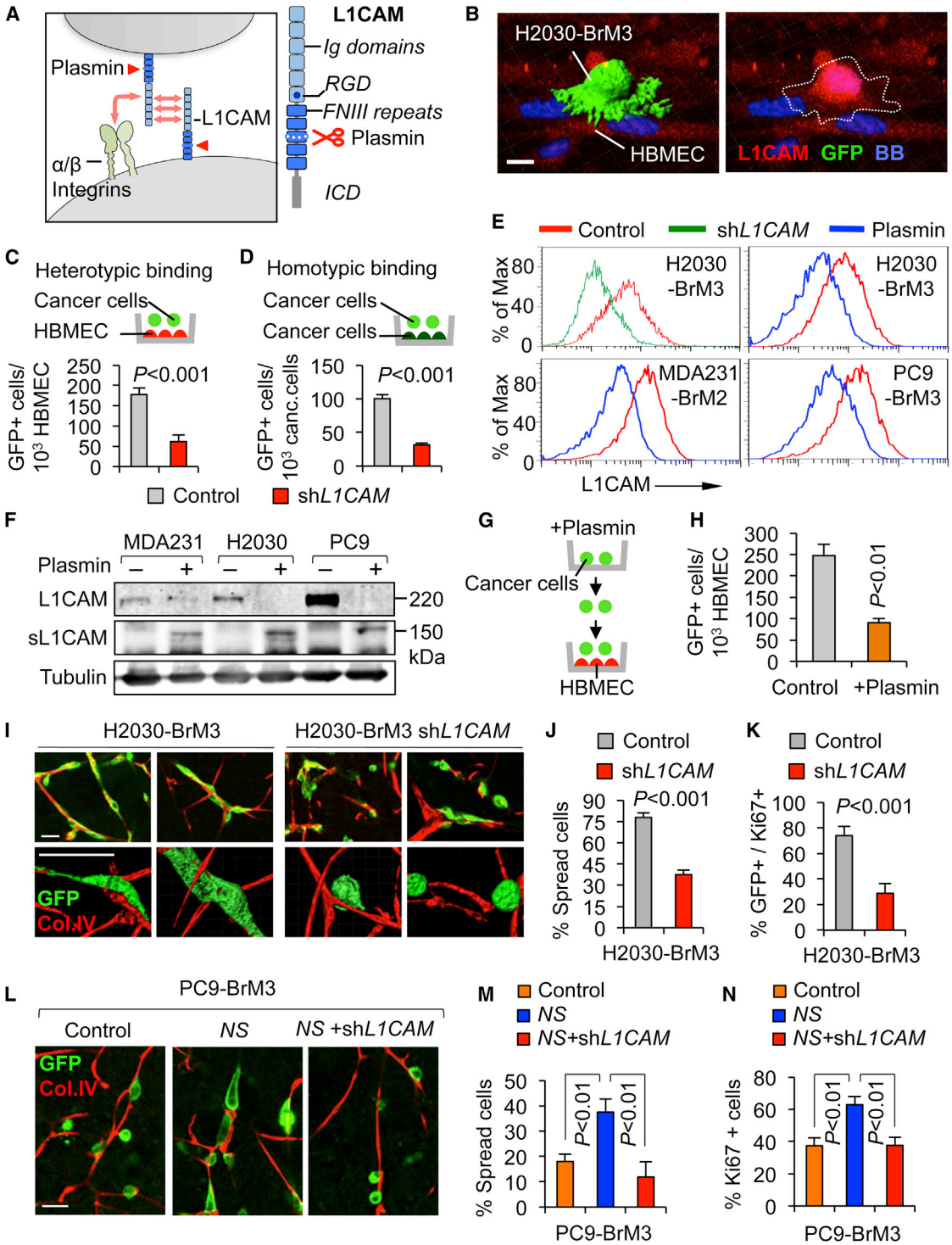

Figure 6. The Plasmin Target L1CAM Mediates Vascular Co-Option by Brain Metastatic Cells

(A) Schema of L1CAM as a mediator of homophilic and heterophilic (e.g., integrins) cell adhesive interactions, and its conversion by plasmin into an adhesion-defective fragment. Ig and fibronectin type III (FNIII) domain repeats, the ICD, and an integrin-binding RGD sequence are indicated.

(B) Suspensions of GFP+ H2030-BrM3 cells were placed on top of a monolayer of HBMECs.

(C and D) Analysis of H2030-BrM3 binding to HBMEC monolayers (C) or H2030-BrM3 monolayers (D), and the effect of L1CAM knockdown. Data are averages ± SEM, n = 5, scoring at least ten fields per coverslip.

(E) Flow cytometry of cell-surface L1CAM in the indicated brain cells expressing *L1CAM* shRNA or incubated with plasmin, compared with untreated controls.

(legend continued on next page)

plasmin can promote cancer cell proliferation and invasion by cleaving growth factor precursors and extracellular matrix proteins (McMahon and Kwaan, 2008), anti-PA serpin levels in tumors and blood are associated with poor outcome in many cancers (Berger, 2002; Foekens et al., 1995; Harbeck et al., 1999). Here we show that anti-PA serpins shield metastatic cells from PA-plasmin in the brain, providing a clear prometastatic advantage.

Averting Fas Killing and Protecting L1CAM Vascular Co-Option

Although FasL plays important roles in immune homeostasis (Krammer, 2000) and is present in tumors (Baldini et al., 2009), its expression is particularly acute in reactive astrocytes (Beer et al., 2000). Astrocytes are the main source of FasL in response to infiltrating leukocytes, and of PAs in response to brain injury. We show that metastasis-associated astrocytes express both PA and FasL. Plasmin releases membrane-bound FasL from astrocytes, and sFasL levels in brain tissue depend on plasmin. Brain metastatic cells from lung or breast cancers suffer Fas-dependent death in the brain unless they are protected by anti-PA serpins. We conclude that Fas signaling mediates and anti-PA serpins prevent the attrition of infiltrating cancer cells in the brain.

We show that L1CAM mediates the spread of metastatic cells on the vasculature and additionally mediates interactions between cancer cells. When cancer cells are experimentally depleted of L1CAM, they fail to co-opt brain capillaries and metastatic outgrowth stalls. Cancer cell-derived anti-PA serpins prevent plasmin destruction of L1CAM, providing yet another benefit besides averting Fas-mediated cancer cell killing. L1CAM expression is normally restricted to neurons, where it mediates axonal guidance through highly plastic interactions of the growth cone with surrounding components (Wiencken-Barger et al., 2004). The dynamic nature of L1CAM adhesive interactions might be particularly advantageous to cancer cells in their quest to co-opt the vasculature while invading tissue. Although the molecular basis for vascular co-option in cancer is largely unknown, the present identification of L1CAM as a mediator provides an opening for a mechanistic dissection of this process.

Implications beyond Brain Metastasis

The molecular mechanisms defined here protect metastatic cells against selective pressures that are particularly acute in the brain. However, a high mortality of infiltrating cancer cells is characteristic of metastasis in general (Gupta and Massagué, 2006; Valastyan and Weinberg, 2011), and vascular co-option occurs in metastasis to other organs and by other types of cancer (Donnem et al., 2013). Vascular co-option also provides cancer cells with an escape from therapy-induced hypoxia (Leenders et al., 2004). The anti-PA serpins that are upregulated in our brain metastatic models are also expressed, albeit at lower levels, in counterparts that are metastatic to other organs. Moreover, L1CAM expression in primary tumors is associated with poor prognosis in various types of cancer, as are PA, plasmin, and FasL. The reactive brain stroma, with its high capacity to generate PA-plasmin and FasL, may be more challenging to infiltrating cancer cells than is the stroma in other organs, and as a result, it may select for accentuated versions of otherwise general metastatic traits. Although anti-PA serpins, plasmin, FasL, and L1CAM have not previously been connected to metastatic cell survival and vascular co-option, their repeated clinical association with poor prognosis and the mechanistic links exposed in the present work may reflect a wider role in cancer than is shown here.

EXPERIMENTAL PROCEDURES

Animal Studies

All animal experiments were done in accordance with a protocol approved by the MSKCC Institutional Animal Care and Use Committee. Athymic NCR nu/nu, Cr:NIH bg-nu-xid, FVB/NCr (all from NCI-Frederick), and B6129SF1/J (The Jackson Laboratory) female mice 4–6 weeks of age were used. Brain metastatic derivatives of a syngeneic ErbB2 model (ErbB2-BrM2) were established according to a previous protocol (Bos et al., 2009; Nguyen et al., 2009) and are detailed in the Extended Experimental Procedures. Brain colonization assays were performed as follows: We injected 100 μl of PBS into the left ventricle containing 50,000 cells (for long-term experiments) or 500,000 cells (for short-term experiments) in the case of MDA231-BrM2a, CN34BrM-2c, H2030-BrM3, and PC9-BrM3, and 100,000 cells in the case of 373N1, 393N1, 482N1, 2691N1, and ErbB2-BrM2. Brain colonization was analyzed in vivo and ex vivo by BLI. Anesthetized mice (ketamine 100 mg/kg/xylazine 10 mg/kg) were injected retro-orbitally with D-Luciferin (150 mg/kg) and imaged with an IVIS Spectrum Xenogen machine (Caliper Life Sciences). Bioluminescence analysis was performed using Living Image software, version 2.50.

Brain Slice Assays

Organotypic slice cultures from adult mouse brain were prepared by adapting previously described methods (Polleux and Ghosh, 2002). Brains from 4- to 6-week-old athymic NCR nu/nu mice were dissected in Hank's balanced salt solution (HBSS) supplemented with HEPES (pH 7.4, 2.5 mM), D-glucose (30 mM), $CaCl_2$ (1 mM), $MgSO_4$ (1 mM), $NaHCO_3$ (4 mM), and embedded in low-melting agarose (Lonza) preheated at 42°C. The embedded brains were cut into 250 μm slices using a vibratome (Leica). Brain slices (bregma −1 mm to +3 mm) were placed with flat spatulas on top of 0.8 μm pore membranes (Millipore) in slice culture media (Dulbecco's modified Eagle's medium [DMEM], supplemented HBSS, fetal bovine serum 5%, L-glutamine (1 mM), 100 IU/ml penicillin, 100 μg/ml streptomycin). The brain slices were incubated at 37°C and 5%

(F) Anti-L1CAM western immunoblotting of cells and culture supernatants after incubation with or without plasmin.
(G and H) Cancer cells were treated with plasmin and subjected to HBMEC adhesion assays. Data are averages ± SEM, n = 3, scoring at least five fields per coverslip.
(I) Control or *L1CAM*-depleted H2030-BrM3 cells after infiltrating brain tissue slices. GFP+ cancer cells (green) and vasculature (collagen IV immunostaining, red) were visualized after 2 days. Two representative images are shown per condition. Bottom: high magnification.
(J and K) Quantification of cells that were spread on capillaries (J) and Ki67+ cells (K) in the experiments of (I). Data are averages ± SEM, n = 6 slices, scoring at least three fields per slice, from two independent experiments.
(L) Effect of NS overexpression and *L1CAM* depletion on the interaction of PC9-BrM3 cells with capillaries in brain slices.
(M and N) Quantification of cells that were spread on capillaries (M) and Ki67+ cells (N) in the experiments shown in (L).
Data are averages ± SEM and quantitated as (J) and (K). All p values by Student's t test. Scale bars, 10 μm (B) and 50 μm (I and L). See also Figure S6.

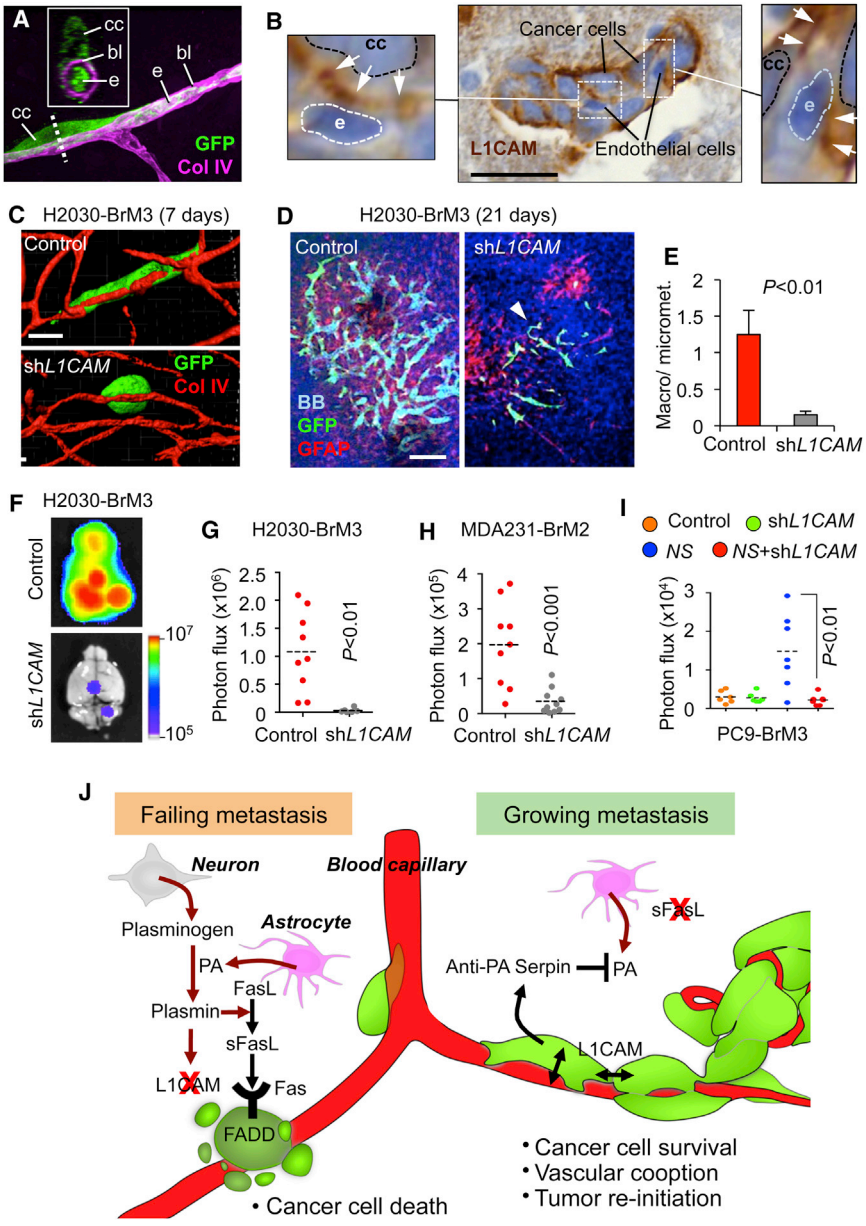

Figure 7. L1CAM Mediates Metastatic Outgrowth in the Brain

(A) GFP+ H2030-BrM3 co-opting the basal lamina rich in collagen IV of endothelial cells labeled with VE-cadherin in brain slices. bl, basal lamina; e, endothelium; cc, cancer cell.

(B) Immunohistochemical staining with anti-L1CAM antibodies and hematoxylin and eosin (H&E) counterstaining of incipient brain colonies formed by H2030-BrM3. Cancer cells (cc, pale blue nuclei) remain close to each other and interact with endothelial cells (e, dark blue nuclei). Insets: higher magnification of cell-cell contact areas.

(C) H2030-BrM3 cells infiltrating the brain 7 days after intracardiac injection, and the effect of *L1CAM* depletion.

(D) Representative images of GFP+ metastatic lesions from brains at 21 days.

(E) Relative abundance of macrometastasis over micrometastasis (as defined in Figure 3F) in brains shown in (D). Number of lesions: control = 283.2 ± 84.8, sh*L1CAM* = 69.8 ± 11.5. Data are averages ± SEM, n = 3 brains.

(F and G) Representative images (F) and quantification (G) of ex vivo brain BLI from mice inoculated with the indicated H2030-BrM3 cells. Control shRNA, n = 9; sh*L1CAM*, n = 6.

(H) Quantification of ex vivo brain BLI from mice that were arterially inoculated with indicated MDA231-BrM2 cells. Control shRNA, n = 9; sh*L1CAM*, n = 10.

(I) Quantification of ex vivo brain BLI from mice that were arterially inoculated with the indicated PC9-BrM3 cells (n = 5–7). All p values were determined by Student's t test. Scale bar, 25 μm (B), 30 μm (C), and 200 μm (D).

(J) Model of the action of the stromal PA-plasmin system against cancer cells that infiltrate the brain, and the role of anti-PA serpins in protecting brain metastatic cells from stromal PA-plasmin. Reactive astrocytes produce PAs in the presence of extravasated cancer cells. Left side: metastasis fails when PAs generate plasmin from neuron-derived plasminogen and plasmin mobilizes FasL from astrocytes to kill cancer cells. Additionally, plasmin cleaves and inactivates L1CAM, a cell adhesion molecule that cancer cells express for vascular co-option. Right side: metastasis proceeds when brain metastatic cells express anti-PA serpins that prevent the generation of plasmin and its deleterious effects on the survival and vascular attachment of the cancer cells.

See also Figure S7.

CO_2 for 1 hr, and then 3 × 10^4 cancer cells suspended in 2 μl of culture media were placed on the surface of the slice and incubated for 48–72 hr. Brain slices could be maintained under these conditions for up to 5 days without apparent alterations in tissue architecture. α2-antiplasmin (2.5 μg/ml; Molecular Innovations), NS, and serpin B2 (0.5 μg/ml each; Peprotech) were added to the medium. sFasL (500 ng/ml; Peprotech) or FasL blocking antibodies (12.5 μg/ml; BD) were added to the medium, and slices were preincubated for 24 hr before addition of cancer cells. Brain slices were fixed in paraformaldehyde (4%) overnight, and then free-floating immunofluorescence was performed for GFP (1:1,000, ref. GFP-1020; Aves Labs), cleaved caspase-3 (1:500, ref. 9661; Cell Signaling), collagen IV (1:500, ref. AB756P; Millipore). Nuclei were stained with Bis-Benzamide (1 μg/ml; Sigma). Slices were mounted with ProLong Gold anti-fade reagent (Invitrogen).

SUPPLEMENTAL INFORMATION

Supplemental Information includes Extended Experimental Procedures and seven figures and can be found with this article online at http://dx.doi.org/10.1016/j.cell.2014.01.040.

ACKNOWLEDGMENTS

We thank A. Boire, P. Bos, L. DeAngelis, E. Holland, and J. Posner for helpful input; the Brain Tumor Center for tumor samples; Marija Drobnjak for establishing the tissue microarray from lung cancer brain metastasis; T. Jacks for cell lines; and A. Thorburn for reagents. This work was supported by NIH grants P01-CA129243 and U54-163167, DOD Innovator award

W81XWH-12-0074, and the Alan and Sandra Gerry Metastasis Research Initiative (J.M.). M.V. is a Hope Funds for Cancer Research postdoctoral fellow. A.C.O. is an Erwin Schrödinger Fellowship awardee (J3013, FWF, Austrian Science Fund). X.H.-F.Z. is a McNair Scholar and the recipient of a grant from the Breast Cancer Research Foundation. J.M. is an investigator of the Howard Hughes Medical Institute.

Received: June 14, 2013
Revised: September 16, 2013
Accepted: January 14, 2014
Published: February 27, 2014

REFERENCES

Adhami, F., Yu, D., Yin, W., Schloemer, A., Burns, K.A., Liao, G., Degen, J.L., Chen, J., and Kuan, C.Y. (2008). Deleterious effects of plasminogen activators in neonatal cerebral hypoxia-ischemia. Am. J. Pathol. *172*, 1704–1716.

Ashkenazi, A., and Dixit, V.M. (1998). Death receptors: signaling and modulation. Science *281*, 1305–1308.

Bajou, K., Peng, H., Laug, W.E., Maillard, C., Noel, A., Foidart, J.M., Martial, J.A., and DeClerck, Y.A. (2008). Plasminogen activator inhibitor-1 protects endothelial cells from FasL-mediated apoptosis. Cancer Cell *14*, 324–334.

Baldini, E., Ulisse, S., Marchioni, E., Di Benedetto, A., Giovannetti, G., Petrangeli, E., Sentinelli, S., Donnorso, R.P., Reale, M.G., Mottolese, M., et al. (2009). Expression of Fas and Fas ligand in human testicular germ cell tumours. Int. J. Androl. *32*, 123–130.

Beer, R., Franz, G., Schöpf, M., Reindl, M., Zelger, B., Schmutzhard, E., Poewe, W., and Kampfl, A. (2000). Expression of Fas and Fas ligand after experimental traumatic brain injury in the rat. J. Cereb. Blood Flow Metab. *20*, 669–677.

Benarroch, E.E. (2007). Tissue plasminogen activator: beyond thrombolysis. Neurology *69*, 799–802.

Berger, D.H. (2002). Plasmin/plasminogen system in colorectal cancer. World J. Surg. *26*, 767–771.

Bos, P.D., Zhang, X.H., Nadal, C., Shu, W., Gomis, R.R., Nguyen, D.X., Minn, A.J., van de Vijver, M.J., Gerald, W.L., Foekens, J.A., and Massagué, J. (2009). Genes that mediate breast cancer metastasis to the brain. Nature *459*, 1005–1009.

Carbonell, W.S., Ansorge, O., Sibson, N., and Muschel, R. (2009). The vascular basement membrane as "soil" in brain metastasis. PLoS ONE *4*, e5857.

Castellani, V., De Angelis, E., Kenwrick, S., and Rougon, G. (2002). Cis and trans interactions of L1 with neuropilin-1 control axonal responses to semaphorin 3A. EMBO J. *21*, 6348–6357.

Chambers, A.F., Groom, A.C., and MacDonald, I.C. (2002). Dissemination and growth of cancer cells in metastatic sites. Nat. Rev. Cancer *2*, 563–572.

Chen, Z.L., and Strickland, S. (1997). Neuronal death in the hippocampus is promoted by plasmin-catalyzed degradation of laminin. Cell *91*, 917–925.

Chinnaiyan, A.M., Tepper, C.G., Seldin, M.F., O'Rourke, K., Kischkel, F.C., Hellbardt, S., Krammer, P.H., Peter, M.E., and Dixit, V.M. (1996). FADD/MORT1 is a common mediator of CD95 (Fas/APO-1) and tumor necrosis factor receptor-induced apoptosis. J. Biol. Chem. *271*, 4961–4965.

Choi, C., and Benveniste, E.N. (2004). Fas ligand/Fas system in the brain: regulator of immune and apoptotic responses. Brain Res. Brain Res. Rev. *44*, 65–81.

Doberstein, K., Wieland, A., Lee, S.B., Blaheta, R.A., Wedel, S., Moch, H., Schraml, P., Pfeilschifter, J., Kristiansen, G., and Gutwein, P. (2011). L1-CAM expression in ccRCC correlates with shorter patients survival times and confers chemoresistance in renal cell carcinoma cells. Carcinogenesis *32*, 262–270.

Donier, E., Gomez-Sanchez, J.A., Grijota-Martinez, C., Lakomá, J., Baars, S., Garcia-Alonso, L., and Cabedo, H. (2012). L1CAM binds ErbB receptors through Ig-like domains coupling cell adhesion and neuregulin signalling. PLoS ONE *7*, e40674.

Donnem, T., Hu, J., Ferguson, M., Adighibe, O., Snell, C., Harris, A.L., Gatter, K.C., and Pezzella, F. (2013). Vessel co-option in primary human tumors and metastases: an obstacle to effective anti-angiogenic treatment? Cancer Med. *2*, 427–436.

Fang, H., Placencio, V.R., and DeClerck, Y.A. (2012). Protumorigenic activity of plasminogen activator inhibitor-1 through an antiapoptotic function. J. Natl. Cancer Inst. *104*, 1470–1484.

Feld, R., Rubinstein, L.V., and Weisenberger, T.H. (1984). Sites of recurrence in resected stage I non-small-cell lung cancer: a guide for future studies. J. Clin. Oncol. *2*, 1352–1358.

Felding-Habermann, B., Silletti, S., Mei, F., Siu, C.H., Yip, P.M., Brooks, P.C., Cheresh, D.A., O'Toole, T.E., Ginsberg, M.H., and Montgomery, A.M. (1997). A single immunoglobulin-like domain of the human neural cell adhesion molecule L1 supports adhesion by multiple vascular and platelet integrins. J. Cell Biol. *139*, 1567–1581.

Foekens, J.A., Look, M.P., Peters, H.A., van Putten, W.L., Portengen, H., and Klijn, J.G. (1995). Urokinase-type plasminogen activator and its inhibitor PAI-1: predictors of poor response to tamoxifen therapy in recurrent breast cancer. J. Natl. Cancer Inst. *87*, 751–756.

Francia, G., Cruz-Munoz, W., Man, S., Xu, P., and Kerbel, R.S. (2011). Mouse models of advanced spontaneous metastasis for experimental therapeutics. Nat. Rev. Cancer *11*, 135–141.

Fujimoto, S., Katsuki, H., Ohnishi, M., Takagi, M., Kume, T., and Akaike, A. (2008). Plasminogen potentiates thrombin cytotoxicity and contributes to pathology of intracerebral hemorrhage in rats. J. Cereb. Blood Flow Metab. *28*, 506–515.

Ganesh, B.S., and Chintala, S.K. (2011). Inhibition of reactive gliosis attenuates excitotoxicity-mediated death of retinal ganglion cells. PLoS ONE *6*, e18305.

Gavrilovic, I.T., and Posner, J.B. (2005). Brain metastases: epidemiology and pathophysiology. J. Neurooncol. *75*, 5–14.

Gupta, G.P., and Massagué, J. (2006). Cancer metastasis: building a framework. Cell *127*, 679–695.

Gutiérrez-Fernández, A., Gingles, N.A., Bai, H., Castellino, F.J., Parmer, R.J., and Miles, L.A. (2009). Plasminogen enhances neuritogenesis on laminin-1. J. Neurosci. *29*, 12393–12400.

Harbeck, N., Thomssen, C., Berger, U., Ulm, K., Kates, R.E., Höfler, H., Jänicke, F., Graeff, H., and Schmitt, M. (1999). Invasion marker PAI-1 remains a strong prognostic factor after long-term follow-up both for primary breast cancer and following first relapse. Breast Cancer Res. Treat. *54*, 147–157.

Heyn, C., Ronald, J.A., Ramadan, S.S., Snir, J.A., Barry, A.M., MacKenzie, L.T., Mikulis, D.J., Palmieri, D., Bronder, J.L., Steeg, P.S., et al. (2006). In vivo MRI of cancer cell fate at the single-cell level in a mouse model of breast cancer metastasis to the brain. Magn. Reson. Med. *56*, 1001–1010.

Irving, J.A., Pike, R.N., Lesk, A.M., and Whisstock, J.C. (2000). Phylogeny of the serpin superfamily: implications of patterns of amino acid conservation for structure and function. Genome Res. *10*, 1845–1864.

Kang, Y., Siegel, P.M., Shu, W., Drobnjak, M., Kakonen, S.M., Cordón-Cardo, C., Guise, T.A., and Massagué, J. (2003). A multigenic program mediating breast cancer metastasis to bone. Cancer Cell *3*, 537–549.

Karrison, T.G., Ferguson, D.J., and Meier, P. (1999). Dormancy of mammary carcinoma after mastectomy. J. Natl. Cancer Inst. *91*, 80–85.

Kienast, Y., von Baumgarten, L., Fuhrmann, M., Klinkert, W.E., Goldbrunner, R., Herms, J., and Winkler, F. (2010). Real-time imaging reveals the single steps of brain metastasis formation. Nat. Med. *16*, 116–122.

Krammer, P.H. (2000). CD95's deadly mission in the immune system. Nature *407*, 789–795.

Kulahin, N., Li, S., Hinsby, A., Kiselyov, V., Berezin, V., and Bock, E. (2008). Fibronectin type III (FN3) modules of the neuronal cell adhesion molecule L1 interact directly with the fibroblast growth factor (FGF) receptor. Mol. Cell. Neurosci. *37*, 528–536.

Law, R.H., Zhang, Q., McGowan, S., Buckle, A.M., Silverman, G.A., Wong, W., Rosado, C.J., Langendorf, C.G., Pike, R.N., Bird, P.I., and Whisstock, J.C. (2006). An overview of the serpin superfamily. Genome Biol. *7*, 216.

Leenders, W.P., Küsters, B., Verrijp, K., Maass, C., Wesseling, P., Heerschap, A., Ruiter, D., Ryan, A., and de Waal, R. (2004). Antiangiogenic therapy of cerebral melanoma metastases results in sustained tumor progression via vessel co-option. Clin. Cancer Res. *10*, 6222–6230.

Li, B., Wang, C., Zhang, Y., Zhao, X.Y., Huang, B., Wu, P.F., Li, Q., Li, H., Liu, Y.S., Cao, L.Y., et al. (2013). Elevated PLGF contributes to small-cell lung cancer brain metastasis. Oncogene *32*, 2952–2962.

Lin, Q.B., Balasubramanian, K., Fan, D., Kim, S.J., Guo, L., Wang, H., Bar-Eli, M., Aldape, K.D., and Fidler, I.J. (2010). Reactive astrocytes protect melanoma cells from chemotherapy by sequestering intracellular calcium through gap junction communication channels. Neoplasia *12*, 748–754.

Lorger, M., and Felding-Habermann, B. (2010). Capturing changes in the brain microenvironment during initial steps of breast cancer brain metastasis. Am. J. Pathol. *176*, 2958–2971.

Maher, E.A., Mietz, J., Arteaga, C.L., DePinho, R.A., and Mohla, S. (2009). Brain metastasis: opportunities in basic and translational research. Cancer Res. *69*, 6015–6020.

Maness, P.F., and Schachner, M. (2007). Neural recognition molecules of the immunoglobulin superfamily: signaling transducers of axon guidance and neuronal migration. Nat. Neurosci. *10*, 19–26.

McMahon, B., and Kwaan, H.C. (2008). The plasminogen activator system and cancer. Pathophysiol. Haemost. Thromb. *36*, 184–194.

Mechtersheimer, S., Gutwein, P., Agmon-Levin, N., Stoeck, A., Oleszewski, M., Riedle, S., Postina, R., Fahrenholz, F., Fogel, M., Lemmon, V., and Altevogt, P. (2001). Ectodomain shedding of L1 adhesion molecule promotes cell migration by autocrine binding to integrins. J. Cell Biol. *155*, 661–673.

Minn, A.J., Gupta, G.P., Siegel, P.M., Bos, P.D., Shu, W., Giri, D.D., Viale, A., Olshen, A.B., Gerald, W.L., and Massagué, J. (2005). Genes that mediate breast cancer metastasis to lung. Nature *436*, 518–524.

Muller, W.J., Sinn, E., Pattengale, P.K., Wallace, R., and Leder, P. (1988). Single-step induction of mammary adenocarcinoma in transgenic mice bearing the activated c-neu oncogene. Cell *54*, 105–115.

Nayeem, N., Silletti, S., Yang, X., Lemmon, V.P., Reisfeld, R.A., Stallcup, W.B., and Montgomery, A.M. (1999). A potential role for the plasmin(ogen) system in the posttranslational cleavage of the neural cell adhesion molecule L1. J. Cell Sci. *112*, 4739–4749.

Nguyen, D.X., Chiang, A.C., Zhang, X.H., Kim, J.Y., Kris, M.G., Ladanyi, M., Gerald, W.L., and Massagué, J. (2009). WNT/TCF signaling through LEF1 and HOXB9 mediates lung adenocarcinoma metastasis. Cell *138*, 51–62.

Pang, P.T., Teng, H.K., Zaitsev, E., Woo, N.T., Sakata, K., Zhen, S., Teng, K.K., Yung, W.H., Hempstead, B.L., and Lu, B. (2004). Cleavage of proBDNF by tPA/plasmin is essential for long-term hippocampal plasticity. Science *306*, 487–491.

Polleux, F., and Ghosh, A. (2002). The slice overlay assay: a versatile tool to study the influence of extracellular signals on neuronal development. Sci. STKE *2002*, p19.

Schäfer, M.K., and Altevogt, P. (2010). L1CAM malfunction in the nervous system and human carcinomas. Cell. Mol. Life Sci. *67*, 2425–2437.

Schröder, C., Schumacher, U., Fogel, M., Feuerhake, F., Müller, V., Wirtz, R.M., Altevogt, P., Krenkel, S., Jänicke, F., and Milde-Langosch, K. (2009). Expression and prognostic value of L1-CAM in breast cancer. Oncol. Rep. *22*, 1109–1117.

Seike, T., Fujita, K., Yamakawa, Y., Kido, M.A., Takiguchi, S., Teramoto, N., Iguchi, H., and Noda, M. (2011). Interaction between lung cancer cells and astrocytes via specific inflammatory cytokines in the microenvironment of brain metastasis. Clin. Exp. Metastasis *28*, 13–25.

Silletti, S., Mei, F., Sheppard, D., and Montgomery, A.M. (2000). Plasmin-sensitive dibasic sequences in the third fibronectin-like domain of L1-cell adhesion molecule (CAM) facilitate homomultimerization and concomitant integrin recruitment. J. Cell Biol. *149*, 1485–1502.

Sofroniew, M.V., and Vinters, H.V. (2010). Astrocytes: biology and pathology. Acta Neuropathol. *119*, 7–35.

Takehara, S., Onda, M., Zhang, J., Nishiyama, M., Yang, X., Mikami, B., and Lomas, D.A. (2009). The 2.1-A crystal structure of native neuroserpin reveals unique structural elements that contribute to conformational instability. J. Mol. Biol. *388*, 11–20.

Teesalu, T., Hinkkanen, A.E., and Vaheri, A. (2001). Coordinated induction of extracellular proteolysis systems during experimental autoimmune encephalomyelitis in mice. Am. J. Pathol. *159*, 2227–2237.

Valastyan, S., and Weinberg, R.A. (2011). Tumor metastasis: molecular insights and evolving paradigms. Cell *147*, 275–292.

Vanharanta, S., and Massagué, J. (2013). Origins of metastatic traits. Cancer Cell *24*, 410–421.

Voura, E.B., Ramjeesingh, R.A., Montgomery, A.M., and Siu, C.H. (2001). Involvement of integrin alpha(v)beta(3) and cell adhesion molecule L1 in transendothelial migration of melanoma cells. Mol. Biol. Cell *12*, 2699–2710.

Wang, X., Haroon, F., Karray, S., Martina Deckert, and Schlüter, D. (2013). Astrocytic Fas ligand expression is required to induce T-cell apoptosis and recovery from experimental autoimmune encephalomyelitis. Eur. J. Immunol. *43*, 115–124.

Wiencken-Barger, A.E., Mavity-Hudson, J., Bartsch, U., Schachner, M., and Casagrande, V.A. (2004). The role of L1 in axon pathfinding and fasciculation. Cereb. Cortex *14*, 121–131.

Winslow, M.M., Dayton, T.L., Verhaak, R.G., Kim-Kiselak, C., Snyder, E.L., Feldser, D.M., Hubbard, D.D., DuPage, M.J., Whittaker, C.A., Hoersch, S., et al. (2011). Suppression of lung adenocarcinoma progression by Nkx2-1. Nature *473*, 101–104.

Yepes, M., Sandkvist, M., Wong, M.K., Coleman, T.A., Smith, E., Cohan, S.L., and Lawrence, D.A. (2000). Neuroserpin reduces cerebral infarct volume and protects neurons from ischemia-induced apoptosis. Blood *96*, 569–576.

EXTENDED EXPERIMENTAL PROCEDURES

Brain Metastatic Cell Isolation and Culture

Human brain metastatic cell lines were previously described (Bos et al., 2009; Nguyen et al., 2009). A ErbB2-P cell line was established from MMTV driven-NeuNT transgenic mammary tumors in mice (Muller et al., 1988). ErbB2-P cells were injected intracardiacally to obtain brain metastatic derivatives. Briefly, a cell suspension containing 10^5 ErbB2-P cells expressing a TK-GFP-Luciferase (TGL) construct, in a volume of 100 μl was injected in the left cardiac ventricle of anesthetized 4–6 week-old FVB/NCr mice. Tumor development was monitored by weekly bioluminescence imaging using the IVIS-200 imaging system from Xenogen as previously described. Brain lesions were localized by ex vivo bioluminescence imaging, and resected under sterile conditions. Tissue was minced and placed in culture medium containing a 1:1 mixture of DMEM/Ham's F12 supplemented with 0.125% collagenase III and 0.1% hyaluronidase. Samples were incubated at room temperature for 4–5 h, with gentle rocking. After collagenase treatment, cells were briefly centrifuged, resuspended in 0.25% trypsin, and incubated for a further 15 min in a 37°C water bath. Cells were resuspended in culture media and allowed to grow to confluence on a 10cm dish. GFP+ cells were sorted for further propagation in culture or inoculation in mice.

MDA231-BrM2, ErbB2-BrM2, 373N1, 393N1, 482N1, 2691N1 where cultured in DME media supplemented with 10% fetal bovine serum (FBS), 2 mM L-Glutamine, 100IU/ml penicillin/streptomycin and 1 μg/ml amphotericin B. CN34-BrM2 were cultured in M199 media supplemented with 2.5% fetal bovine serum (FBS), 10 μg/ml insulin, 0.5 μg/ml hydrocortisone, 20 ng/ml EGF, 100 ng/ml cholera toxin, 1 μg/ml amphothericin B, and 100 U/ml penicillin/streptomycin. H2030-BrM3 and PC9-BrM3 were cultured in RPMI1640 media supplemented with 10% fetal bovine serum (FBS), 2 mM L-Glutamine, 100IU/ml penicillin/streptomycin, and 1 μg/ml amphotericin B. For retrovirus and lentivirus production, GPG29 and 293T cells, respectively, were cultured in DME media supplemented with 10% fetal bovine serum (FBS), 2 mM L-Glutamine, 100 IU/ml penicillin/streptomycin, and 1 μg/ml amphotericin B. In addition the GPG29 media contained 0.3 mg/ml G418, 20ng/ml doxycycline and 2 μg/ml puromycin. MDA231-BrM2 SCP were prepared by serial dilution as previously shown (Kang et al., 2003) and cultured in DME media supplemented with 10% fetal bovine serum (FBS), 2 mM L-Glutamine, 100IU/ml penicillin/streptomycin, and 1 μg/ml amphotericin B. Mouse microglia cells were acquired at ATCC (CRL-2467). Mouse astrocytes were obtained from two-day old pups (Schildge et al., 2013). In brief, brains were mechanically dissociated, filtered through 100 μm filters and cell suspension cultured in a petri dish under normal conditions during the next 10 days. On day 10, the dish was incubated overnight at 37°C with gentle shaking. Next day media was changed and astrocyte enrichment confirmed with > 90% of cells staining positive for GFAP.

Gene-Expression Analysis

Whole RNA was isolated from cells using RNAeasy Mini Kit (QIAGEN). 1,000 ng RNA was used to generate cDNA using Transcriptor First Strand cDNA synthesis kit (Roche). Gene expression was analyzed using Taqman gene expression assays (Applied Biosystems). Assays used for human genes: *FADD* (Hs04187499_m1), *FASL* (Hs00181225_m1), *L1CAM* (Hs01109748_m1), *SERPINB2* (Hs00234032_m1), *SERPIND1* (Hs00164821_m1), *SERPINE1* (Hs01126604_m1), *SERPINE2* (Hs00385730_m1), *SERPINI1* probe#1 (Hs01115397_m1), *SERPINI1* probe#2 (Hs01115400_m1). Assays used for the mouse genes: *fasL* (Mm00438864_m1), *serpinb2* (Mm00440905_m1), *serpind1* (Mm00433939_m1), *serpine2* (Mm00436753_m1), *serpinI1* (Mm00436740_m1). Relative gene expression was normalized to the "housekeeping" genes namely *β2M* (Hs99999907_m1) and *β2 m* (Mm00437762_m1). Quantitative PCR reaction was performed on ABI 7900HT Fast Real-Time PCR system and analyzed using the software SDS2.2.2 (Applied Biosystems).

Clinical Samples and Immunohistochemistry

Thirty-three and 123 cases from lung and breast cancer brain metastasis respectively were obtained from the Brain Tumor Center and the Department of Pathology at MSKCC. Paraffin embedded tissue microarrays from brain metastases obtained from breast and lung cancer were obtained from the MSKCC Department of Pathology in compliance with protocols approved by the MSKCC Institutional Review Board (IRB). Immunohistochemistry for Neuroserpin (Abcam, ab16171-100, Lot number 158358, 1:250), SerpinB2 (Santa Cruz, sc-25745, Lot number L1406, 5 μg/ml), and L1CAM (Covance, SIG-3911, Lot number D13BF00437, 1 ug/ml) were performed by the MSKCC Molecular Cytology Core Facility using standardized automated protocols. Immunoreactivity stainings were evaluated and scored by clinical pathologists (J.T.H., E.B.) in a blinded fashion. 42 brain metastasis samples from breast cancer were annotated for the primary tumor type, corresponding to 27 cases positive for neuroserpin and 12 for serpin B2. Analysis of expression of *SERPINB2* and *SERPINI1* was performed by using the MSKCC data set #1 (Nguyen et al., 2009), including 107 samples of which 106 had clinical information available. The hazard ratio of the average value of *SERPINI1* and *SERPINB2* was computed based on Cox Proportional Hazards Models, as implemented by the "coxph" command in R.

Plasmids, Recombinant Proteins, and In Vitro Experiments

Human Neuroserpin cDNA (Open Biosystems) was subcloned into the pBABE-puro retroviral expression vector. Site directed mutagenesis (Stratagene) was performed to generate the Δloop mutant previously characterized (Takehara et al., 2009). TRC number for shRNAs used in this study are Neuroserpin (TRCN0000052356 and TRCN0000052355), SERPINB2 (TRCN0000052278), SERPIND1 (TRCN 0000052226), SERPINE2 (TRCN 0000052317), L1CAM (TRCN0000063916). All shRNAs were specific against the human

gene and expressed in pLKO.1-shRNA vectors (Open Biosystems) with Puromycin, Hygromycin or Neomycin (G418) resistance genes. The *ST6GalNaC5* shRNA was previously described (Bos et al., 2009). The FADD-DD construct was kindly provided by Andrew M. Thornburn and subcloned in a pLVX-hygro lentiviral expression vector. Neuroserpin ELISA was performed following manufacturer's instructions (Peprotech). DVL-K chromogenic assays were performed by plating $5x10^4$ cells in 24 well plates and starvation in DMEM FBS 0.25% overnight. Plasminogen (Molecular innovations, 0.125 μM) was added to cancer cells that were incubated for 24 hr prior to DVL-K chromogenic assays. D-VLK chromogenic substrate (Molecular Innovations) was prepared following manufacturer's instructions. D-VLK was added to cells and a change in absorbance was monitored at 405 nm. For (3-(4,5-dimethylthiazolyl-2-yl)-2,5-diphenyltetrazolium bromide (MTT) cell proliferation assays, 5×10^2 cells were plated in 96 well plates, and for cleaved Caspase-3, $25x10^3$ cells were plated in 24-well plates, starved with FBS 0.25% overnight in presence or absence of sFasL (Peprotech, 100–500 ng/ml) and incubated for the indicated period of time. Plasmin (Molecular Innovations) treatment of cells was done at 1.6 U/ml for 4 hr.

Immunofluorescence

Tissue for immunofluorescence was obtained after overnight fixation with PFA 4% at 4°C. Slicing of the brain was done by using a vibratome (Leica) or sliding microtome (Fisher). Both types of brain slices (250 μm and 80 μm respectively) were blocked in NGS 10%, BSA 2%, Triton 0.25% in PBS for 2 hr at room temperature (RT). Primary antibodies were incubated overnight at 4C in the blocking solution and the following day for 30 min at RT. After extensive washing in PBS-Triton 0.25%, the secondary antibody was added in the blocking solution and incubated for 2 hr. After extensive washing in PBS-Triton 0.25%, nuclei were stained with Bis-Benzamide for 7 min at RT. Primary antibodies: GFP (Aves Labs, ref. GFP-1020, 1:1,000), Plasminogen (Santa Cruz, ref. sc-25546, 1:100), tPA (Molecular Innovations, ref. ASMTPA-GF, 1:50), uPA (Molecular Innovations, ref. ASMUPA-GF, 1:50), GFAP (Dako, ref. Z0334, and Millipore, ref. MAB360, both 1:1,000), Ibal (Wako, ref. 019-19741, 1:500), Col.IV (Millipore, ref. AB756P, 1:500), NeuN (Millipore, ref. MAB377, 1:500), Neuroserpin (Abcam, ref. ab16171, 1:250), FasL (Santa Cruz, ref. sc-834 and sc-6237, 1:100), L1CAM (Millipore, ref. CBL275, 1:200 and Covance, ref. SIG-3911, 1 μg/ml). Secondary antibodies: Alexa-Fluor anti-chicken^{488}, anti-rabbit^{555}, anti-mouse^{555}, anti-mouse^{633} (Invitrogen).

Immunoblotting

Cell pellets were lysed with RIPA buffer and protein concentrations were determined by BSA Protein Assay Kit (Pierce). Proteins were separated by SDS-PAGE and transferred to nitrocellulose membranes or PVDF membranes. Membranes were immunoblotted with antibodies against FAS (Santa Cruz, ref. sc-715, 1:100), FasL (Santa Cruz, ref. sc-834 and sc-6237 1:100), L1CAM (Millipore, ref. CBL275, eBioscience, ref. 14-1719, and Abcam, ref. ab24345, 1: 200–1,000), FLAG (Sigma, 1:2,000), Serpin B2 (Abcam, ref. 47742, 1:500), Tubulin (Cell signaling, 1:2,000).

Confocal Microscopy and Image Analysis

Images were acquired with a Leica SP5 up-right confocal microscope 10X, 20X, 40X and 63X objectives and analyzed with ImageJ, Imaris and Metamorph softwares. In brain slice assays, GFP+ cell bodies that were located > 40 μm from the surface of the slice were considered for analysis in order to avoid cells clusters remaining on the surface. ImageJ was used to determine the spread cell index by using confocal images and applying the round filter with a 0.45 treshold.

In Vitro Blood-Brain Barrier Assay

This assay was performed as previously described (Bos et al., 2009). Briefly, primary human umbilical vein endothelial cells (HUVEC, ScienCell) were cocultured with human primary astrocytes (ScienCell), on opposite sides of a polylysine-treated, gelatin-coated tissue culture transwell insert for 3 days. In brief, 3 μm pore PET tissue culture inserts (Fisher) were treated with polylysine (1 μg/ml, Millipore) overnight, washed four times, and coated with 0.2% gelatin (Sigma) for a minimum of 30 min. Inserts were placed upside-down in a 15 cm plate, and 10^5 primary human astrocytes were plated on the membrane surface. Astrocytes were fed every 15 min for 5 h, and the inserts were then flipped and placed in 24-well plates. $5x10^5$ endothelial cells were plated on the upper chamber of the inserts, and cultures were placed in the incubator, without further perturbation. For BBB transmigration assays, $5x10^5$ cells were seeded on the upper chamber and incubated for 14–18 h. Inserts were washed with PBS and fixed with 4% PFA for 20 min. The membranes were removed from the plastic insert, immunofluorescence against GFP was performed and mounted on a microscope slide. Pictures of multiple fields from 5–8 inserts per experiment were taken, and the number of transmigrated cells was counted.

Flow Cytometry

Monolayers of adherent cells were detached using 1 mM EDTA, resuspended in single-cell suspensions and incubated with fluorochrome-conjugated monoclonal antibodies of human L1CAM (eBioscience, ref. 12-1719-42). The cell surface expression of L1CAM was analyzed by a FACSCalibur flow cytometer (BD Biosciences).

Cell Adhesion Assays

HBMEC or tumor cells were plated in 2-well culture slides (BD Falcon) and allowed to grow over 90% confluent. Tumor cells were labeled with CellTracker Green CMFDA (5-Chloromethylfluorescein Diacetate) (Molecular Probes). 7.2×10^4 prelabeled tumor cells

were allowed to adhere to the monolayer of cancer cells for 20 min. After washing off the nonadherent cells, the slides were fixed with 1% paraformaldehyde and mounted with mounting medium with DAPI (Vector Labs). Adherent cells (green) and the nucleus of total cells (blue) were scored by fluorescence microscopy. The number of GFP+ cancer cells adhered to HBMEC or cancer cells covering the bottom of every well was calculated.

SUPPLEMENTAL REFERENCES

Bai, H., Baik, N., Kiosses, W.B., Krajewski, S., Miles, L.A., and Parmer, R.J. (2011). The novel plasminogen receptor, plasminogen receptor(KT) (Plg-R(KT)), regulates catecholamine release. J. Biol. Chem. *286*, 33125–33133.

Schildge, S., Bohrer, C., Beck, K., and Schachtrup, C. (2013). Isolation and culture of mouse cortical astrocytes. J. Vis. Exp. *pii*, 50079.

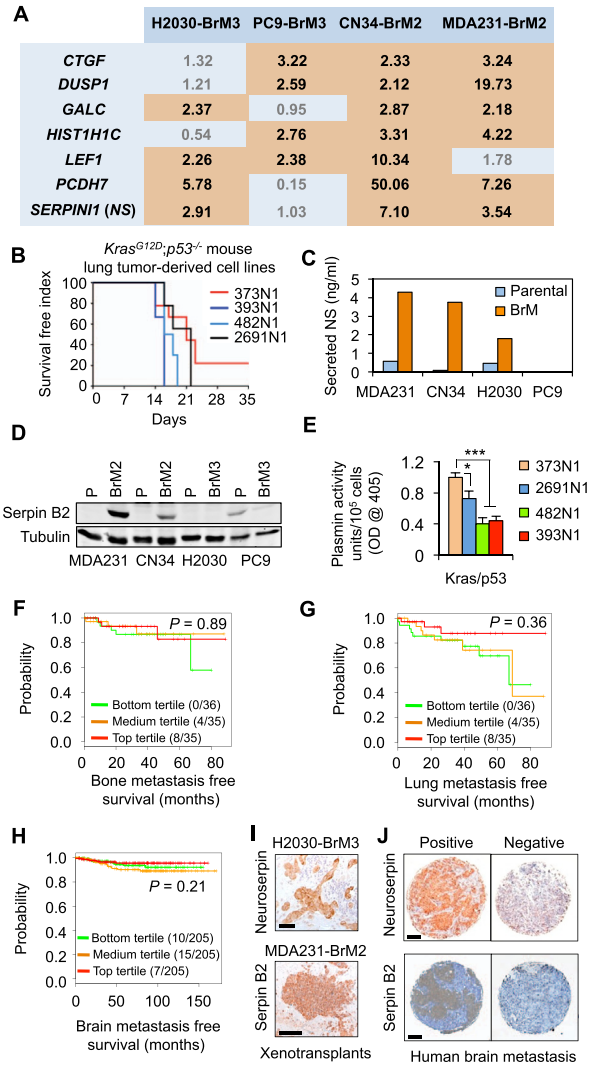

Figure S1. Highly Expressed Genes in Brain Metastasis Models and Clinical Samples, Related to Figure 1

(A) Genes that were previously associated with brain metastatic activity in two lung adenocarcinoma brain metastasis models (H2030-BrM3 and PC9-BrM3; Nguyen et al., 2009) or two breast cancer brain metastasis models (MDA231-BrM2 and CN34-BrM2; Bos et al., 2009) and found to be shared among these models. Values indicate fold-increase in the expression of these genes in BrM cells compared to non-brain metastatic counterparts in GeneChip transcriptional data sets (Nguyen et al., 2009, Bos et al., 2009).

(B) Cell lines derived from genetically engineered *Kras*^{G12D};*p53*$^{-/-}$ mouse lung tumors (373N1, 393N1, 482N1, 2691N1) were tested for overall metastatic activity from the arterial circulation in syngeneic mice. Kaplan-Meier plots of metastasis-free survival, n = 10 mice per cell line. All cell lines showed multiorganic metastatic activity as previously described (Winslow et al., 2011), but differed in brain metastatic activity (see Figure 1).

(C) Neuroserpin (NS) protein levels in low-serum cell culture supernatants, as determined by ELISA.

(D) Serpin B2 (SB2) protein levels in cell lysates determined by western immunoblotting.

(E) Plasminogen conversion into plasmin was inhibited to different extents by cell culture supernatants from the indicated cells lines. Plasmin activity was determined by a chromogenic assay (Bai et al., 2011). p values were determined by Student's t test. *p < 0.05, ***p < 0.001.

(F and G) Kaplan-Meier analysis of bone metastasis-free survival and contralateral lung metastasis-free survival in 106 cases of lung adenocarcinoma classified based on *SERPINB2* and *SERPINI1* mRNA levels in the primary tumor. p value calculated by a Cox proportional hazard model, with *SERPINB2* and *SERPINI1* expression treated as a continuous variable.

(H) Kaplan-Meier analysis of brain metastasis-free survival in 615 cases of breast adenocarcinoma (EMC-MSK data set) classified based on *SERPINB2* and *SERPINI1* mRNA levels in the primary tumor. p value calculated from a Cox proportional hazard model, with *SERPINB2* and *SERPINI1* expression treated as a continuous variable.

(I) Immunohistochemistry against NS and SB2 in brains from mice intracardiacally inoculated with indicated cell lines.

(J) Representative brain metastasis tissue microarray cores stained with neuroserpin or serpin B2 antibodies.

Scale bar, 100 μm.

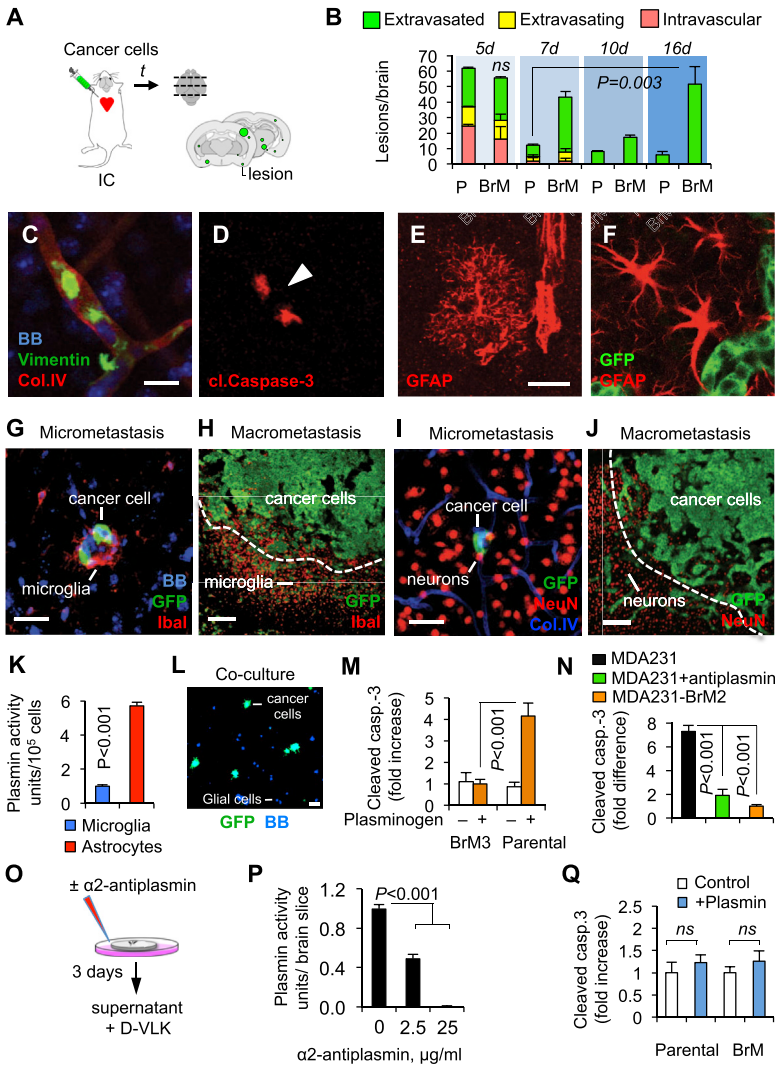

Figure S2. Interactions of Metastatic Cells with the Brain Parenchyma, Related to Figure 2

(A) Experimental design for the analysis of brain metastatic colonies formed by circulating cancer cells.

(B) Quantification of parental MDA231 (P) and MDA231-BrM2 (BrM) cells in the brain at the indicated times after inoculation into the arterial circulation of mice. Data are averages ± SEM of multiple fields in 2 brains. p values were determined by Student's t test comparing cells extravasated in the parental and brain metastatic populations before and after 7 days.

(C and D) Cells (vimentin+, green) that remained in the lumen of brain capillaries (collagen IV positive) 7 days after inoculation scored positive for cleaved caspase-3 immunofluorescence (red, arrowhead in D).

(E and F) Nonreactive astrocytes (E), located in uninvolved areas and reactive astrocytes in areas that contain metastatic cells (F) can be distinguished based on dramatic morphological changes, including modified interaction with capillaries, and the thickening and reduction in the number of cellular processes.

(G–J) Interaction of H2030-BrM3 cells with different components of the brain microenvironment including reactive microglia (Iba1+) and neurons (NeuN+) from extravasation through overt metastasis.

(K) D-VLK chromogenic plasmin substrate assay was used to compare the plasmin activity associated with mouse microglia or astrocyte culture supernatants.

(L) Representative image of low-density cocultures of cancer cells and glial cells.

(M) Quantification of cleaved caspase-3 positive cancer cells in cocultures with glial cells with added plasminogen. Values are normalized to H2030-BrM3 without plasminogen, and are averages ± SEM n = 6–9 cocultures per condition, scoring multiple fields per coculture, from 3 independent experiments.

(N) Quantification of cleaved caspase-3 positive cancer cells in brain slice assays. Values are normalized to MDA231-BrM2, and are averages ± SEM n = 6–10 brain slices, from 2 independent experiments.

(O) Schema of experimental design to analyze plasmin activity in brain slices.

(P) α2-antiplasmin inhibition of plasmin in brain slices.

(Q) Plasmin addition to H2030 cells in monolayer culture does not induce cell death.

All p values were determined by Student's t test. Scale bars, 10 μm (C), 50 μm (E, F, L), 20 μm (G and I), 500 μm (H and J).

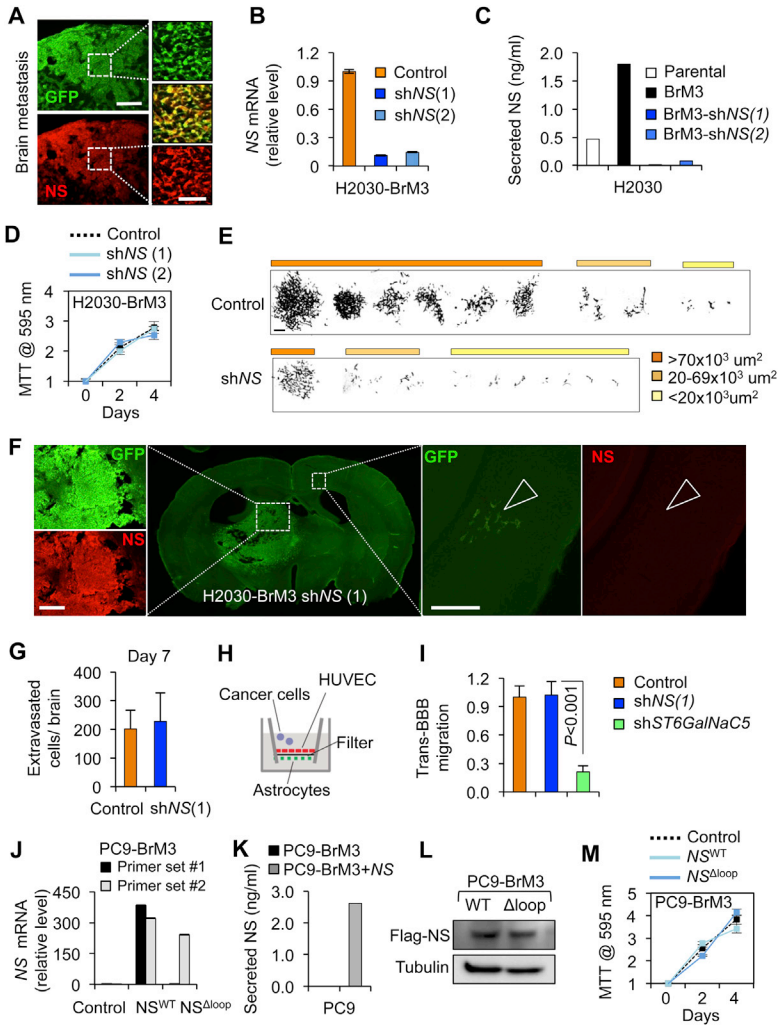

Figure S3. Neuroserpin Mediates Brain Metastasis by Lung Cancer Cells, Related to Figure 3

(A) Neuroserpin IF (red) in brains harboring GFP+ H2030-BrM3 metastasis (green). Insets show colocalization (yellow) of neuroserpin with GFP+ cancer cells.

(B) *Neuroserpin* mRNA levels as determined by qRT-PCR in H2030-BrM3 and derivatives transduced with *neuroserpin* shRNAs.

(C) Neuroserpin ELISA was performed on culture supernatants of the indicated H2030 derivatives.

(D) MTT cell proliferation assays of H2030-BrM3 cells transduced with control or *NS* shRNA.

(E) Tracings and size distribution of metastatic lesions in the brain of animals from Figure 3D. Relative abundance of each size group is shown for every experimental condition.

(F) The few macrometastases that were formed by *neuroserpin*-depleted H2030-BrM3 cells scored positive for neuroserpin IF (left), whereas micrometastases scored negative for neuroserpin (right).

(G) *Neuroserpin* knockdown in H2030-BrM3 did not alter the number of extravasated cells on day 7 after inoculation. Data are averages ± SEM from 3 brains.

(H) Schema of the assay for cancer cell transmigration through an experimental blood-brain barrier (BBB) (Bos et al., 2009). HUVEC, primary human umbilical vein endothelial cells.

(I) Quantification of cells that migrated through this experimental BBB normalized to H2030-BrM3 control cells. An shRNA targeting the brain extravasation mediator *ST6GalNaC5* (Bos et al., 2009) served as positive control (sh*NS* versus sh*ST6GalNaC5*, $p < 0.001$). At least 5 independent migration assays were performed for each condition.

(J) qRT-PCR analysis of *neuroserpin* mRNA levels in PC9-BrM3 cells that were transfected with the indicated flag epitope-tagged neuroserpin constructs. PCR primer set #1 recognizes only the wild-type *neuroserpin* mRNA, whereas set #2 recognizes both the wild-type and the Δloop mutant forms.

(K) Neuroserpin ELISA was performed on culture supernatants of PC9-BrM3 or this cell line expressing a neuroserpin cDNA.

(L) Anti-flag western immunoblotting of culture supernatants from PC9-BrM3 cells expressing the indicated neuroserpin constructs. Tubulin immunoblotting was used as loading control.

(M) Proliferation assays of control and neuroserpin overexpressing PC9-BrM3 cells.

All p values by Student's t test. Scale bars, 200 μm (A and F), 100 μm (A, inset), 250 μm (E).

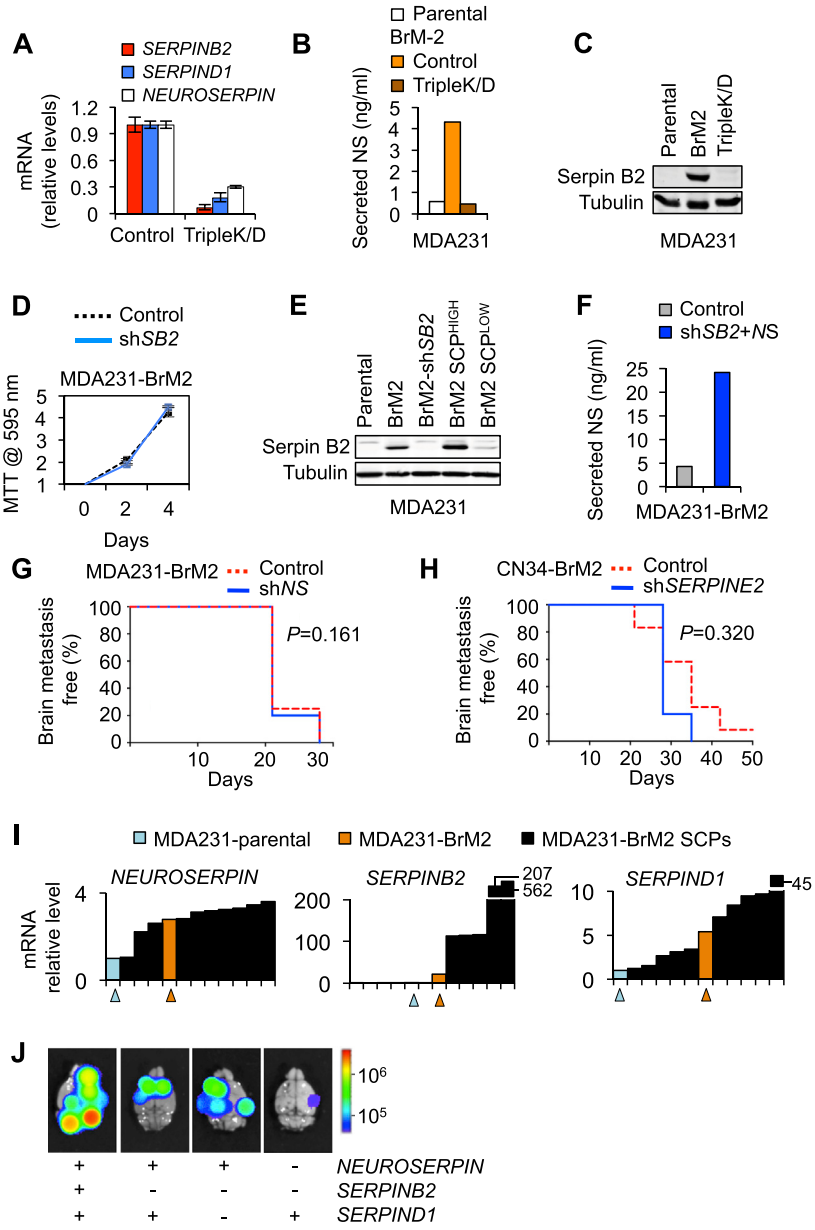

Figure S4. Analysis of Multiple Coexpressed Serpins in MDA231-BrM2 Cells, Related to Figure 4

(A) qRT-PCR of MDA231-BrM2 expressing shRNAs that target the three indicated serpins.

(B) Neuroserpin ELISA in low serum culture supernatant from the indicated cell lines.

(C) Anti-serpin B2 (SB2) western immunoblotting of lysates from the indicated cell lines.

(D) Proliferation assays of sh*SB2* MDA231-BrM2 transduced cell lines.

(E) Anti-serpin B2 western immunoblotting of lysates from the indicated cells lines. BrM2-SCP^{HIGH} and BrM2-SCP^{LOW} correspond to clonal lines from MDA231-BrM2 as shown in Figure 4D.

(F) Neuroserpin ELISA of culture supernatant from the indicated cell lines.

(G) Kaplan–Meier plot of brain metastasis-free survival comparing MDA231-BrM2 control (n = 5) and sh*NS* (1) (n = 9). p values by log rank Mantel-Cox test.

(H) Kaplan–Meier plot of brain metastasis-free survival comparing CN34-BrM2 control (n = 12) and sh*SERPINE2* (1) (n = 5) were analyzed. p values by log rank Mantel-Cox test.

(I) qRT-PCR analysis of serpin expression in single-cell progenies (SCP) isolated from the MDA231-BrM2 cell line. Black, clonal lines; blue, parental population; orange, BrM population.

(J) Ex vivo BLI images of representative brains from metastasis assays of MDA231-BrM2 SCP expressing the indicated serpins quantified in Figure 4D.

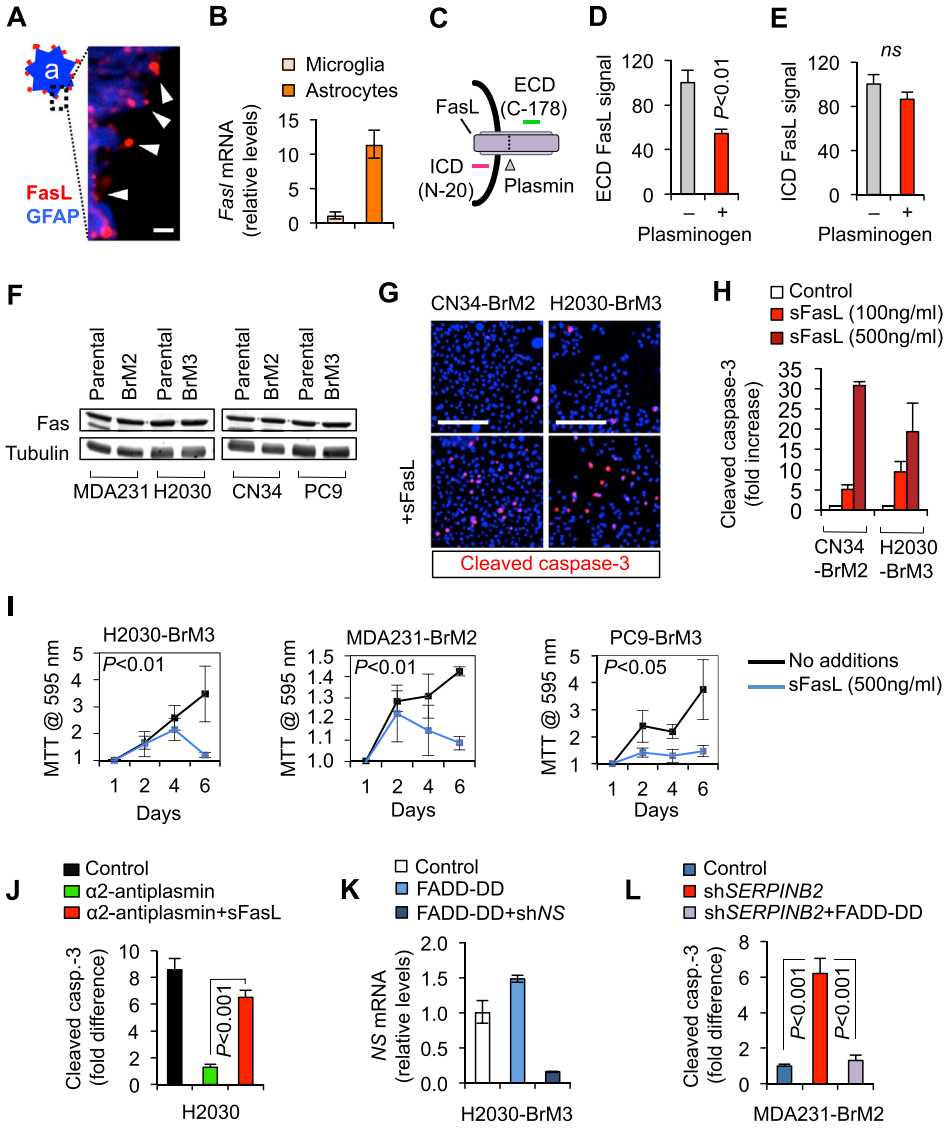

Figure S5. sFasL Triggers Apoptosis in Brain Metastatic Cells, Related to Figure 5

(A) High magnification of an astrocyte stained with anti-GFAP and anti-FasL antibodies in a brain lesion formed by H2030-BrM3 cells.

(B) qRT-PCR analysis of *FasL* mRNA levels in primary cultures of mouse astrocytes and microglia. Data are averages of triplicates ± SEM.

(C) Schema showing the various anti-FasL antibodies used. (D and E) Quantification of FasL ECD and ICD immunofluorescence signals in Figure 5C.

(F) Anti-Fas western immunoblotting of indicated cell lysates. Tubulin immunoblotting was used as loading control.

(G) Cleaved caspase-3 IF (red) in breast (CN34-BrM2) and lung (H2030-BrM3) brain metastatic cell monolayers that were incubated with or without addition of sFasL (500ng/ml). Blue, nuclear staining.

(H) Quantification of the experiment shown in (G), at the indicated concentrations of sFasL. Data are averages ± SEM of three independent experiments. All differences with control were $p < 0.01$, as determined by Student's t test.

(I) Cell proliferation assays of the indicated cell lines with or without addition of sFasL (500ng/ml). Data are averages of triplicates ± SEM. p values were determined for the difference on day 6, by Student's t test.

(J) Quantification of cleaved caspase-3 positive H2030 cancer cells in brain slices treated with added α2-antiplasmin, α2-antiplasmin and sFasL, or no additions. Values are normalized to H2030+ α2-antiplasmin, and are averages ± SEM n = 5–8 brain slices, scoring at least two fields per slice, from at least 2 independent experiments.

(K) qRT-PCR analysis of *neuroserpin* mRNA levels in H2030-BrM3 cells that were transduced with FADD-DD and *neuroserpin* shRNA vectors as indicated.

(L) Quantification of cleaved caspase-3 positive MDA231-BrM2 cancer cells in brain slices. MDA231-BrM2 cells were transduced with a control vector, serpin *B2* (*SB2*) shRNA, or this shRNA plus a FADD-DD expression vector. Values are normalized to MDA231-BrM2 control, and are averages ± SEM n = 6–10 brain slices, scoring at least two fields per slice, from at least two independent experiments. All p values by Student's t test.

Scale bars, 1 μm (A), 100 μm (G).

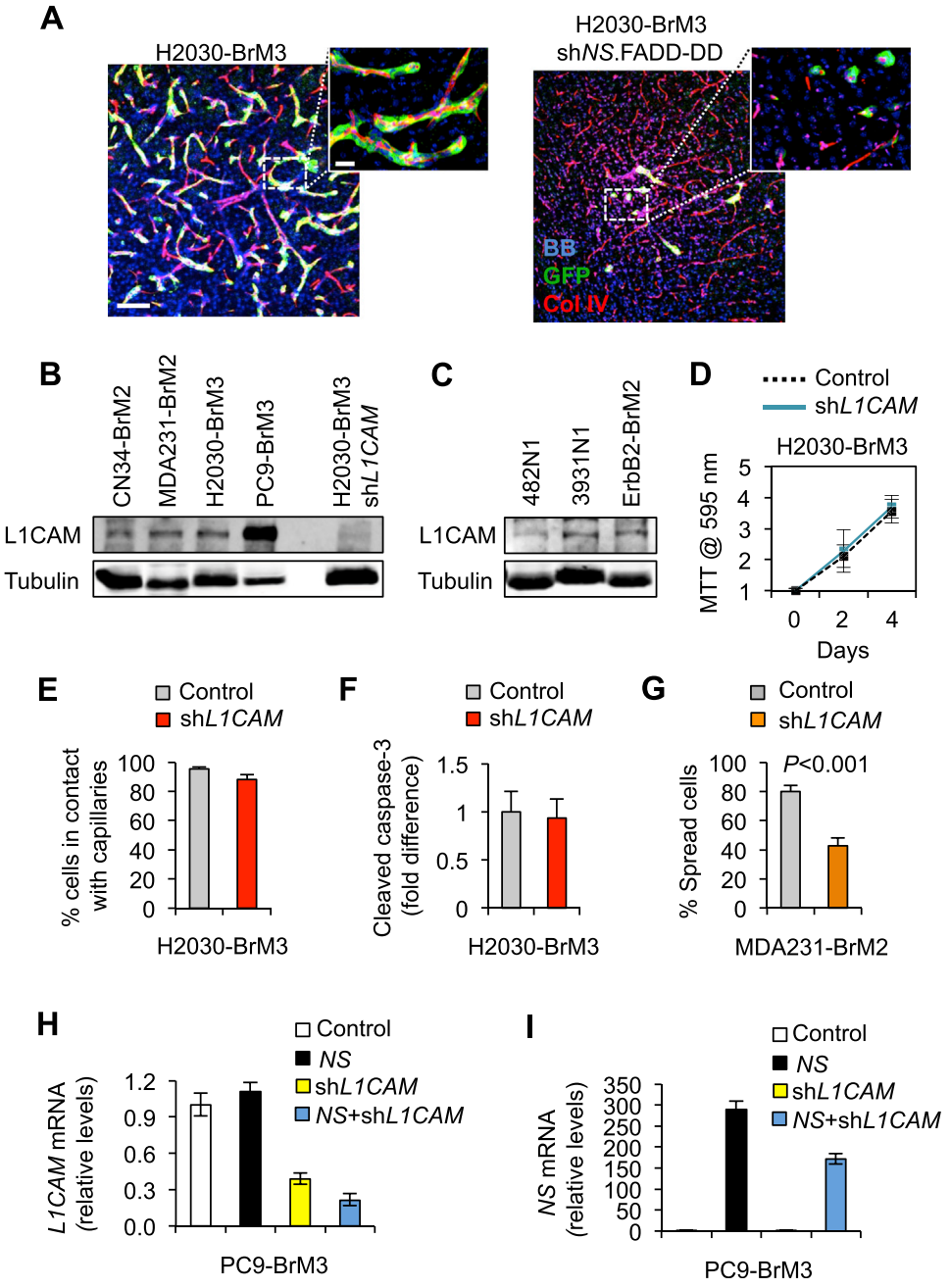

Figure S6. L1CAM as a Plasmin Target and a Mediator of Brain Metastasis, Related to Figure 6

(A) Representative GFP IF images from brains harboring lesions formed by the indicated cell lines. Scale bar, 100 μm, 25 μm (insets). (B and C) Anti-L1CAM western immunoblotting of cell lysates for the indicated human (B) and murine (C) lung or breast cancer cell lines.

(D) MTT proliferation assay of control and *L1CAM*-depleted H2030-BrM3 cells.

(E) Quantification of GFP+ cancer cells that were in contact with, but not necessarily spread on brain capillaries in the experiments of Figure 6I. Ten fields (>180 individual cells) were scored per condition. Data are averages ± SEM.

(F) Quantification of apoptotic wild-type or *L1CAM*-depleted H2030-BrM3 cells in brain slice assays. Data are averages ± SEM n = 5-8 slices from two independent experiments, and at least two fields were scored per slice.

(G) Quantification of MDA231-BrM2 control or sh*L1CAM* transduced cells that were spread on capillaries. Data are averages ± SEM n = 6 slices, scoring at least three fields per slice, from 2 independent experiments. (H,I) qRT-PCR analysis of *L1CAM* (H) and *neuroserpin* (I) mRNA levels in PC9-BrM3 cells that were transduced with neuroserpin expression vector and/or *L1CAM* shRNA vector as indicated.

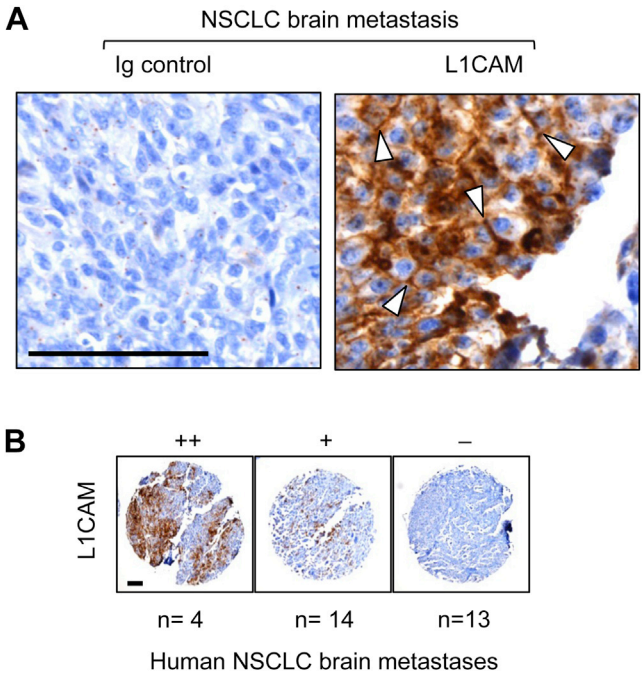

Figure S7. L1CAM Expression in Human Brain Metastases, Related to Figure 7

(A) Representative brain metastasis tissue microarray cores from NSCLC cases stained with anti-L1CAM antibodies. Arrowhead: cell interfaces. Scale bar, 100 μm.

(B) Twenty-nine NSCLC brain metastasis samples were scored as ++ (high), + (low), or - (undetectable), according to the content of L1CAM-positive cells. The number of samples scoring in each level is indicated at the bottom of the panel.